Science and Technology of Welding and Joining

In-situ analysis of the strain evolution during welding using low transformation temperature filler materials

--Manuscript Draft--

Manuscript Number:	STW4710R1
Full Title:	In-situ analysis of the strain evolution during welding using low transformation temperature filler materials
Short Title:	In-situ analysis of the strain evolution during welding using low transformation temperature filler materials
Article Type:	Research Article
Keywords:	Low transformation temperature filler materials; Dilution; Phase transformation; multi-pass welding; GMAW; Strain; Synchrotron diffraction; ADXRD
Corresponding Author:	Jonny Dixneit, Dipl.-Wirt.-Ing. BAM Bundesanstalt fur Materialforschung und -prüfung Berlin, Berlin GERMANY
Corresponding Author Secondary Information:	
Corresponding Author's Institution:	BAM Bundesanstalt fur Materialforschung und -prüfung
Corresponding Author's Secondary Institution:	
First Author:	Jonny Dixneit, Dipl.-Wirt.-Ing.
First Author Secondary Information:	
Order of Authors:	Jonny Dixneit, Dipl.-Wirt.-Ing.
	Florian Vollert
	Arne Kromm
	Jens Gibmeier
	Andreas Hannemann
	Thomas Kannengießer
	Torben Fischer
Order of Authors Secondary Information:	
Abstract:	Compared to conventional welding consumables using low transformation temperature filler materials is an innovative method to mitigate tensile residual stresses due to delayed martensite transformation of the weld. For the effective usage of LTT filler materials a deeper understanding of the complex processes that lead to the final residual stress state during multi pass welding is necessary. Transformation kinetics and the strain evolution of multi-pass welds during welding were investigated in situ at the beamline HEMS@PETRAIII, Germany. Compared to conventional welds the total strain was reduced and compression strain was achieved when using LTT filler materials. For an optimal use of the LTT effect in the root of multi-pass welds the alloying concept must be adapted taking care of dilution.
Funding Information:	

In-situ analysis of the strain evolution during welding using low transformation temperature filler materials

Jonny Dixneit[1], Florian Vollert[2], Arne Kromm[1], Jens Gibmeier[2], Andreas Hannemann[1], Torben Fischer[3], Thomas Kannengiesser[1]

[1]*Bundesanstalt für Materialforschung und -prüfung (BAM), Unter den Eichen 87, 12205 Berlin, Germany*

[2]*Karlsruhe Institute of Technology (KIT), Institute for Applied Materials (IAM), Engelbert-Arnold-Straße 4, 76131 Karlsruhe, Germany*

[3]*Helmholtz-Zentrum Geesthacht (HZG), Institute of Materials Research, Max-Planck-Str. 1, 21502 Geesthacht, Germany*

Jonny Dixneit, jonny.dixneit@bam.de

In-situ analysis of the strain evolution during welding using low transformation temperature filler materials

Compared to conventional welding consumables using low transformation temperature (LTT) filler materials is an innovative method to mitigate tensile residual stresses due to delayed martensite transformation of the weld. For the effective usage of LTT filler materials a deeper understanding of the complex processes that lead to the final residual stress state during multi-pass welding is necessary. Transformation kinetics and the strain evolution of multi-pass welds during welding were investigated in situ at the beamline HEMS@PETRAIII, Germany. Compared to conventional welds the total strain was reduced and compression strain was achieved when using LTT filler materials. For an optimal use of the LTT effect in the root of multi-pass welds the alloying concept must be adapted taking care of dilution.

Keywords: Low transformation temperature filler materials; Dilution; Phase transformation; Multi-pass welding; GMAW; Strain; Synchrotron diffraction; ADXRD

Introduction

Increasing demands on the integrity of welded components led to special focus on base material *(BM)* selection and material-specific design, e.g. in steel industry. Using high-strength low-alloy steels wall thicknesses are reduced as well as remarkable weight savings and lower processing costs are achievable. Unfortunately, HSLA are sensitive to residual stresses due to their limited ductility. The residual stress condition of a welded structure depends on thermal, metallurgical as well as mechanical factors **[1]**. The combination of high hardness, low ductility and tensile residual stresses makes the welded joint susceptible to cold cracking **[2]** while life time expectancy appears unimproved under certain circumstances **[3]**.

Stresses during welding and subsequent cooling are induced due to the localized heat input. Based on this the resulting residual stress state is affected by the interaction

of local hindered shrinkage (restraint) of the weld and the heat affected zone *(HAZ)* as well as due to phase transformations. First concepts about the formation of welding residual stress were based on simple qualitative linear superposition of those factors. For example, basic principles of the impact of weld phase transformations on the stress development were already discussed by Nitschke-Pagel and Wohlfahrt **[4]**. Following this approach, during cooling the yield strength of the austenite phase limits the formation of high shrinkage induced tensile stresses at this stage. As phase transformation of the weld starts compressive stresses are induced due to hindered volume expansion. The amount of compressive stresses increases with decreasing phase transformation temperature as the yield strength of martensite increases too. After the phase transformation has finished tensile stresses may develop again due to hindered shrinkage of the weld during cooling to ambient temperature. This was already proven by the experiment of Jones and Alberry **[5]**, where simple heating trials of different materials have shown different levels of stress depending on the phase transformation temperatures. Nevertheless, these simple models do not allow to predict or to interpret the phase specific residual stress formation in complex multi-pass welds. This becomes important when dealing with residual stress engineering in welding.

Beside the application of post-weld treatments specific control of the welding stresses by means of martensite phase transformation becomes a practical meaning by so called Low Transformation Temperature (*LTT*) filler materials **[6-8]**. LTT alloys are a smart approach of an in-situ-control of the stress development during fusion welding. The idea is to reduce tensile residual stresses or even to induce compressive residual stresses already during the welding cycle by delayed martensitic phase transformation which compensates for thermal stresses **[9]**. Therefore, these alloys exhibit considerable reduced martensite-start-temperatures (M_s) and high yield strengths through tailored

chemical compositions. This allows controlling the stress development in welded joints as already shown for small scale samples **[10-12]**. Specific research on LTT alloys with adapted M_s revealed that the existence of compressive residual stresses due to LTT is not to be generalized. The boundary conditions have significant effects on the level and distribution of residual stresses in welded joints, too. Beside the type of weld (i.e. butt weld, fillet weld) the heat input is most important **[13, 14]**. Moreover, differences occur between longitudinal and transverse residual stress distributions as well as between the surface and the bulk of the weld **[15, 16]**. In some cases even unexpected high tensile residual stress values were observed **[17]**.

In addition, the local microstructure have a large impact on the resulting residual stresses. As certain amounts of austenite are likely to remain due to unfinished martensite formation, residual stresses in both phases must be considered **[18]**. Residual stress measurements using diffraction or mechanical methods (e.g. contour method or incremental hole drilling) allow for accurate evaluation of the residual stresses in LTT welded joints. But these ex-situ techniques do not provide an insight into the mechanisms of stress formation during welding and subsequent cooling. In-situ techniques are required for time and temperature resolved analyses. In particular diffraction techniques using high energy synchrotron X-rays are well suited in the present case as they exclusively permit non-destructive spatial and temporal resolved access to the phase specific strain development and monitoring of phase transformation kinetics.

In-situ diffraction studies dealing with the phase transformation kinetics and the strain evolution of LTT welds based on the main alloying elements chromium *(Cr)* and nickel *(Ni)* have already been reported by the authors **[19-22]**. After first investigations including simple heating and cooling of LTT alloys, re-melting of the welds was

realized by Gas Tungsten Arc Welding *(GTAW)* using a special sample geometry at different beamlines featuring varying experimental conditions. As a result, phase transformation kinetics as well as the strain development were directly observable during the re-melting process. It was concluded that during cooling the austenite exhibits tensile strain longitudinal as well as normal to the welding direction. This is most pronounced in the bulk of the weld. In contrast to this, the martensitic phase shows compressive strain longitudinal to the welding direction while in normal direction tensile strain was observed. Varying heat conduction may be responsible for different strains in both directions. The results clearly illustrate the necessity of time and spatial resolved measurements. Ideally, the time resolution reflects the temperature gradient. The experiments reported up to now just simplified the welding process. Furthermore, welding specific features such as varying thermal cycles caused by multi-pass welding as well as realistic restraint conditions must be included to reproduce the stress-strain formation properly. Especially the restraint intensity, which represents a measure for the hindered shrinkage of the weld due to the stiffness of the joint surrounding, affects the residual stress formation considerably **[23-25]**. Therefore the latest publication by the authors dealt with the influence of the global restraint on the strain evolution during Gas Metal Arc Welding *(GMAW)* in multi-pass welds using energy-dispersive X-ray diffraction *(EDXRD)* **[22]**. Despite a very high intensity of restraint, it was possible to induce compressive strains in case of the LTT CrNi welds, while the conventional weld remains in tension. This was most pronounced in longitudinal direction. Furthermore, the investigations indicated that the phase transformation kinetics depend on the decomposition of the weld metal based on the welding build-up.

While the current publications about LTT alloys often deal with the effect of the interpass temperature on the residual stresses in multi-pass welds **[14, 26-27]**, in this

work the phase and strain formation in multi-pass welding of LTT welds were observed under realistic restraints by means of angle-dispersive X-ray diffraction *(ADXRD)*. In contrast to the EDXRD measurements, the statistics were expected to be improved by evaluating the entire diffraction ring when using ADXRD. Therefore, we focused on in-situ determination of the local and the temporal strain evolution of LTT multi-pass welds by means angular dispersive high energy synchrotron X-ray diffraction. In addition to the usual alloying approach based on the main alloying elements Cr and Ni, LTT weld filler materials based on Cr and manganese *(Mn)* are considered, which are expected to exhibit a lower hot crack susceptibility in contrast to the Cr/Ni weld fillers.

Experimental

Time as well as spatial resolved angle dispersive high energy synchrotron X-ray diffraction measurements during GMAW were performed in transmission geometry at the High Energy Material Science beamline *(HEMS)* at PETRA III (DESY), Hamburg (Germany) **[28]**, see Figure 1. The sample was positioned perpendicular to the primary beam. 2D Diffraction signals were measured using a digital X-ray flat panel detector (Perkin Elmer XRD1621). Measuring parameters are listed in Table 1.

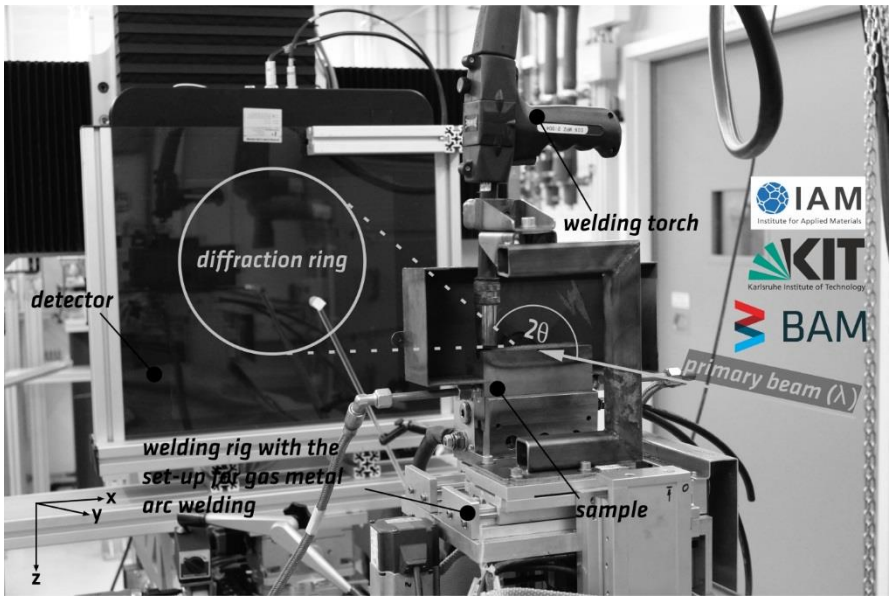

Figure 1: Test set-up for in-situ diffraction studies using synchrotron X-rays during multi-pass welding (GMAW) at the P07 beamline at PETRA III@DESY, Hamburg; the beam path is shown schematically (gray)

To realize GMAW directly at the beam line a mobile and compact welding rig was used. The setup has two parallel translation axes, carrying a GMAW torch and the weld sample mounted on one axis each. A third axis perpendicular allows the vertical adjustment of the whole set-up (z axis, see Fig. 1). For alignment of the z axis the welding rig offers an accuracy of 100 µm achieved by using computer numerically controlled *(CNC)* servo-motors. All positioning and welding procedures take place by remote control as the experiments must be executed in the instrument hutch of the HEMS beamline.

Table 1: Measuring parameters of the angle dispersive x-ray diffraction experiment (ADXRD)

Primary beam cross-section	1 × 1 mm²
Energy / Wave length primary beam	100 keV / 0.012398 nm
Measuring mode	transmission
Measuring frequency	2 Hz (during welding) / 0,5 Hz (during cooling down)
2θ	0 – 15°
Distance between sample and detector	1100 mm
Max. Field of view of the detector	409.6 mm × 409.6 mm
Lattice planes	austenite: {200}, {220}, {311}; ferrite / martensite: {200}, {211}, {220};
temperature at measuring stop (measured by means of thermocouples)	70 °C

Sample geometry

Fusion bead-on-plate welding was performed using a sample geometry providing a high intensity of restraint transverse to the weld direction. As the working area at the beam line is limited but a high intensity of restraint would require large sample dimensions, a special sample geometry was designed, see Fig. 2 (left). A solid block with an U-shaped

gap was used to ensure a high stiffness of the weld surrounding. The dimensions of the gap made it possible to realize three passes between the fillets, see Fig. 2 (right). Those fillets with a width of 10 mm act as a support plate while they were reinforced by the solid block below the weld to ensure a high intensity of restraint as known from large scale samples or specific weld tests **[29]**. The intensity of restraint of this U-shaped sample was already calculated by numerical simulation from R_{Fy} = 40 kN × mm^{-1} × mm^{-1} to $R_{Fy,total}$ = 65 kN × mm^{-1} × mm^{-1} depending on each welded pass. **[30]**.

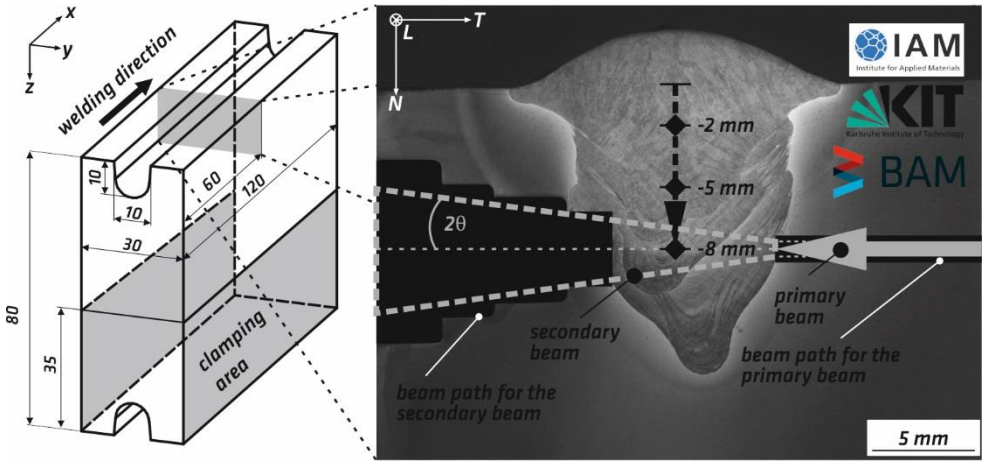

Figure 2: Isometric view of the sample with dimensions given in millimeter before welding (left) and cross section of the gauge area after GMA welding of the final pass (third layer), i.e. measuring position in a depth of -8 mm (right)

In order to obtain the diffraction information from the weld metal exclusively, drill holes for the primary and secondary beam paths were made horizontally into the fillets (Fig. 2 right). Loss of intensity due to attenuation effects could be kept to a minimum this way. On the secondary side the hole-diameter was increased stepwise in order to account for the extension of the diffraction cones. This preparation was done at three different measuring depths (-2 mm, -5 mm and -8 mm) from the weld top surface, which represent the center of the three deposited passes each. Consequently, diffraction

information was obtained from these positions. As the drill holes for the primary and secondary beam paths covered a large portion of the sample, for each sample only one specific measuring depth could be realized. Hence, for every local, temporal resolved strain evolution determined by means of this diffraction approach one specific sample must be used. This procedure further guarantee that the same cooling behavior of each welding layer can be provided and that unwanted heating of the welding rig between the individual synchrotron experiments can be avoided. The other welding layers were fabricated in advance of the beam time in the laboratory using the same welding parameters. This procedure allows for cooling to ambient temperature in each case and ensures complete martensite formation of the welding layers.

In detail the measuring strategy is as follows: By means of an automated GMAW process, three layers (root pass, filler pass and final pass) of the filler material used were deposited into the U-shaped gap as shown in Figure 2. During each welding process the diffraction gauge volume was positioned stationary at one of the three measuring positions in the bulk of the weld. Simultaneously, the lattice strain and the phase fraction evolution was studied during GMAW and cooling either in the currently welded pass or in one of the underlying layers. In the present work we will only focus on the strain development in longitudinal direction of the root pass (measuring position -8 mm) as well as the final pass (measuring position -2 mm) after they were deposited each.

Material and welding parameters

Investigations in this work focused on two selected LTT fillers compared to a conventional filler material for high strength steels *i.e. G Mn4Ni2CrMo* **[31]**. Table 2 shows their chemical compositions and some relevant mechanical properties as the 0.2% proof stress $R_{p0.2}$ and the ultimate tensile strength R_m. Furthermore the martensite

start temperature (M_s) and the bainite start temperature (B_s) are provided as measured by means of dilatometry. The LTT alloys differ in their alloying concept. One follows the well-known Cr/Ni filler approach after **[6]**. The other one uses an alternative composition with Mn substituting Ni **[15]**. With respect to the intended application for low alloyed high strength steels, S960QL **[32]** was used as base material *(BM)*. The welding parameters are shown in Table 3. No preheating was applied. Since the wire diameters of the experimental LTT filler materials differ from the conventional filler material, a comparability of the results was ensured by the same heat input. This means, that the welding parameters differ between the LTT welds and the conventional welds.

For proper assessment of the in-situ diffraction data local information of temporal temperature distributions are essential. In this regard temperature measurements were conducted in each weld pass during separate weldments using thermocouples (type K). The measuring positions were chosen similar as to the location of the diffraction gauge volumes, i.e. -2 mm, -5 mm and -8 mm below the weld top surface by hot dipping of the thermocouples through the primary beam hole (Fig. 2, right). Additionally, at the middle of the sample (x = 60 mm) thermocouples were hot dipped from the top into the melt during deposition of each pass. Using those measurements the temperature gradient was assessable over the welds cross section through modelling of the welding process. The FE model applied for this purpose is described in **[30]**. Based on the heat input and the experimentally determined temperatures, the respective temperature distributions in the measuring depths z = -2 mm, z = -5 mm and z = -8 mm could be determined numerically at intervals of 1 mm over the welds cross section. FE revealed that the transversal temperature gradient is negligible during cooling. Hence, the measured temperatures are assumed to be representative for each location of the diffraction analysis.

Table 2: Chemical composition in wt% and material properties of the base and filler materials. $R_{p0.2}$ and R_m are the 0.2% proof stress and the ultimate tensile strength, respectively. M_s is the martensite start temperature and B_s the bainite start temperature.

Chemical comp. (wt.%),								$R_{p0,2}$	R_m	M_s	B_s
	C	Ni	Cr	Mn	Si	Mo	Fe	MPa	MPa	°C	°C
BM (S960QL)	0.17	0.94	0.49	0.87	0.3	0.52	Bal.	985	1018	419	560
LTT CrNi	0.04	10	10	0.7	0.4	-	Bal.	927	1121	230	-
LTT CrMn	0.08	0.02	11	6.4	0.25	-	Bal.	(-)*	1335	123	-
conventional	0.13	2.19	0.37	1.53	0.8	0.6	Bal.	954	1246	≥ 400	-
M_S, B_S measured in dilatometry test at the base material and pure weld metals *not determinable, because of no distinctive yield point, elastic area too small											

Table 3: welding parameters of the GMAW process applied for each pass

	LTT CrNi	LTT CrMn	conventional
Wire diameter	1.6 mm		1.2 mm
Voltage	30.8 V		36.8 V
Mean current	343 A		345 A
Welding speed	0.37 m × min^{-1}		0.45 m × min^{-1}
Heat input	1.7 kJ × mm^{-1}		
Contact tube distance	18 mm		16 mm
Preheat- and interpass temperature	ambient temperature		
$t_{8/5}$-time (averaged)	12 s		
Welding length	100 mm		
Shielding gas	M21 (82% argon, 18% carbon dioxide)		

Data treatment

With the experimental set-up used, diffraction rings of the lattice planes {200}, {211} and {220} of the martensite phase (α') and the {200}, {220} and {311} of the austenite phase (γ) were evaluated using the open-source software "Fit2D" **[33-34]**. Using this software allows for integrating the Debye-Scherrer-rings that have been recorded with a 2D-detector in azimuthal direction φ. For the phase analysis the complete rings (φ = 0° - 360°) were integrated to obtain a one-dimensional profile of the intensity as a function of 2θ. For the strain analysis a circle segment with an azimuthal angle Δφ = 15° were defined for the longitudinal as well as normal direction according to the weld (see Fig. 3, right). A Pearson-VII-fit was performed for each diffraction peak. By weighting the integrated intensities, $I^{\{hkl\}}$, and using physical factors, ($R^{\{hkl\}}$) **[35-39]**, it is possible to calculate the phase fractions of the austenite (v_γ) and martensite ($v_{\alpha'}$)

based on Equations (1) and (2) with an assumption that only those two phases are present **[40-41]**.

$$v_\gamma = \frac{1}{\left[1 + \left(\frac{I_{\alpha'}^{\{hkl\}}}{I_\gamma^{\{hkl\}}} \times \frac{R_\gamma^{\{hkl\}}}{R_{\alpha'}^{\{hkl\}}}\right)\right]} \quad (1)$$

$$v_{\alpha'} = 1 - p_\gamma \quad (2)$$

Based on Bragg's law and using Equation (3) the lattice spacings were determined for the strain analysis.

$$a_{i,hkl} = d_{hkl}\sqrt{h^2 + k^2 + l^2} \quad (3)$$

A phase specific unit cell parameter was determined by weighting the unit cell parameter $a_{i,hkl}$ with the weight factor f_{hkl} according to Daymond [39].

$$f_{hkl} = P_{hkl} m_{hkl} \frac{E_{hkl}}{E} \quad (4)$$

With the texture factor $P_{hkl} = 1$ as the Debye-Scherrer-rings were fully occupied. From that the phase specific unit cell parameter (a_i) was estimated as a function of temperature. To calculate the elastic lattice strain an unstrained lattice parameter $a_{0,i}$ was determined for each phase. Therefore stress-relieved combs were taken directly from the middle of separate welded samples (x = 60 mm) using identical welding parameters. In accompanying dilatometer tests the phase specific coefficients of thermal expansion α_i were determined for each alloy investigated. Using these values for α_i a temperature (T) dependent unstrained unit cell parameter ($a_{0,i}$) was calculated for the martensite phase and the austenite phase using Equation (5). The elastic lattice strains of the martensite phase (α') and the austenite phase (γ) were calculated using Equation (6). The total elastic lattice strain (ε_t) was calculated by weighting the elastic lattice strains of the martensite phase ($\varepsilon_{\alpha'}$) and the austenite phase (ε_γ) by their accordant phase fractions $V_{\alpha'}$ and V_γ using Equation (7). The error propagation of the fit error was determined and always smaller than 1×10^{-5} (in strain).

$$a_{0,i} = \alpha_i \times \Delta T;\ \text{i … phase} \quad (5)$$

$$\varepsilon_{i_j} = \frac{a_{i_j}(T) - a_{0,i}(T)}{a_{0,i}(T)};\ \text{i … phase, j … principal direction} \quad (6)$$

$$\varepsilon_{t_j}(T) = \varepsilon_{\alpha'_j}(T) \times \mathrm{v}_{\alpha'}(T) + \varepsilon_{\gamma_j}(T) \times \mathrm{v}_{\gamma}(T);\ \text{j … principal direction} \quad (7)$$

Miscellaneous

Electron probe micro analyses (EPMA) were performed over the welds cross section using line scans in the final pass (-2 mm) and in the root pass (-8 mm). For sample preparation in the last step of the procedure the welds cross sections were oxide-polished (particle size 0.25 µm). Table 4 shows the parameter of the EPMA. For the investigation of the local microstructure, samples of the weld cross section were extracted using electrical discharge machining. After embedding, grinding and polishing the samples were etched with Lichtenegger and Bloech etchant (100 ml distilled water, 20 g $(NH_4)HF_2$ and 0.5 g $K_2S_2O_5$) at a temperature of 35°C.

Table 4: Measuring parameters of the electron probe micro analyses (EPMA)

Accelerating voltage	15 kV
Probe current	20 nA
Diameter of the electron beam	spot
Step size	250 µm
Analyzer	JEOL-micro probe JXA-8900 RL

Results and Discussion

Microstructure

The microstructure of the welds consists of martensite or bainite and some retained austenite in case of the LTT welds (Fig. 3). Welding of the final pass led to grain refinement in the root due to multiple heating **[42]**. All passes of the solidified regions of the weld exhibit a cellular structure according to the heat flow in normal direction to the weld. Hardness mappings confirmed that the root of the LTT CrMn welds becomes

tempered slightly (below 500 HV 0.1) while welding of the final pass (up to 570 HV 0.1) resulting in hardness gradients towards the HAZ. In contrast to the LTT CrMn weld the conventional weld (380 HV 0.1) and the LTT CrNi weld (460 HV 0.1) exhibit a homogeneous hardness distribution through the whole weld.

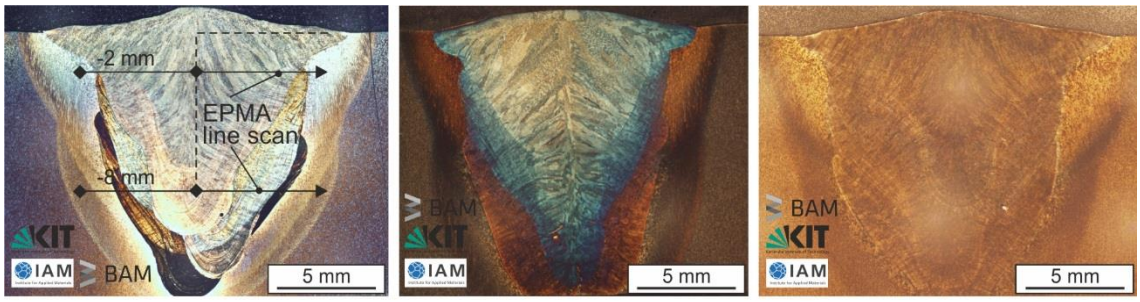

(a) weld „LTT CrMn“ (b) weld „LTT CrNi“ (c) weld „conventional“

Figure 3: Cross section of the joints after welding of the final pass for all three weld consumables investigated here; etched with Lichtenegger and Bloech etchant

As dilution between the LTT welds and the BM was expected additional Electron Probe Micro Analyses (EPMA) were performed at the measuring depths of the in-situ diffraction experiment marked in Fig. 3 (a) using line scans. Measurements of the chemical composition across the welds revealed that the distribution of the main alloying elements Cr, Ni and Mn is characterized by micro segregations **[43-44]**. Applying the approach of Steven & Haynes **[45]** allows for an estimation of the M_s and B_s as a function of the main alloying elements. The M_s based on the EPMA analysis across the welds is given in Fig. 4. M_s varies corresponding to the chemical gradient due to dilution with the BM in case of the LTT welds. The distribution of M_s for the conventional weld is unremarkable at 430 °C while B_s remains constant at 560°C and is not shown. In case of LTT CrNi M_s is 245 °C in average across the final pass and the root. M_s for the LTT CrMn is in average around 120 °C. Nevertheless, both root welds are characterized by a higher scattering of the data (up to about +100K). Therefore,

locally higher M_s temperatures are expected when welding the root. The transition from the weld metal into the HAZ shows in both cases an abrupt rise of M_s. A M_s of about 420 °C was calculated independent of the LTT weld metal.

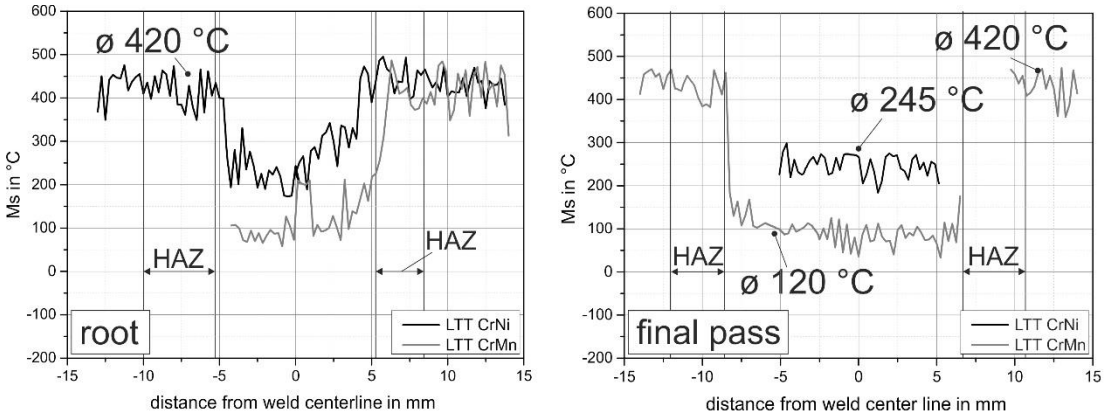

Figure 4: M_s distribution over the cross section of the root (-8 mm; left) and of the final pass (-2 mm, right) of LTT CrNi weld and the LTT CrMn weld based on EPMA analyses of the chemical composition and the empirical approach of Steven and Haynes **[45]**; average temperatures (Ø) of the welds and HAZ were shown in the figure

Martensite and bainite formation

From the graphs presented in Fig. 5, showing the phase fraction vs. the temperature during cooling down, the local changes of the courses can be assigned to phase transformations, hence, indicating M_s and B_s. By this means the formation of martensite (α') and bainite (α_b) during cooling of the root passes (left) and of the final passes (right) of the LTT weld metals as well as for the conventional weld metal after deposition is indicated, hence, when M_s and B_s can be assigned the final microstructure consists of bainite and martensite plus retained austenite. In case of root welding the first α diffraction signals of the conventional weld started to appear already above 550 °C. Those first signals are likely to be related to the formation of bainite. During cooling α' appears subtly at about 420 °C. At ambient temperature in sum about 95% of α_b and α' were formed. For both LTT-fillers the α' phase started to appear also at about

420 °C. No bainite formation was observed. As the observed M_s matches well with the estimation following Steven & Haynes based on the EPMA analyses it is assumed that the local change in slope at about 420 °C stemmed from the transition area into the HAZ which is part of the gauge volume.

A saturation, i.e. an almost horizontal course of the graph, was found when 7% - 10% α' were formed. The characteristic M_s of the LTT CrNi weld metal was then situated at around 360 °C while M_s of LTT CrMn was found at about 327 °C. These temperatures correspond with the maximum variance of M_s calculated by Steven & Haynes (Fig. 4). During further cooling the martensite phase fraction development was comparable between the LTT welds CrNi and CrMn until ambient temperature was reached. Finally, in both cases around 95% of martensite similar to the conventional filler material was formed. Worth mentioning the maximum formation rate of α', i.e. a change in phase fraction vs. temperature change that is indicated by the slope of the graph, was reached at a value of 55% independent from the filler material used.

Comparable to the root α_b and α' phase fraction of the conventional weld started to increase from already about 550 °C for the final pass. An additional change in slope became visible at around 380 °C. While the first inflection point corresponds to the known formation of bainite, the second one is assumed to belong to martensite. After cooling to ambient temperature about 92% of α_b and α' phases were formed. The same accounts for the amount of α' phase of LTT CrNi. Here, solely martensite starts to appear at 210 °C. LTT CrMn shows an M_s of approximately 170°C. Both temperatures are fairly comparable to the analytical estimation (Fig. 4). It is interesting that LTT CrMn martensite was formed more rapidly compared the LTT CrNi. While 50% of martensite of the latter were formed in a temperature range of $\Delta T = 70$ °C, the LTT CrMn had formed the same amount of martensite already in a range of $\Delta T = 50$ °C. The

amounts of retained austenite at ambient temperature are below 10% for the conventional wire and LTT CrNi, respectively below 17% of LTT CrMn.

In summary, the LTT fillers show lower M_s temperatures than the conventional filler material, as expected. In case of the LTT root welds dilution with the BM induces a shift of M_s to higher temperatures compared to the nominal values. Nevertheless, the martensite formation is virtually completed at ambient temperature. Less dilution is observed for the final pass. Here, M_s of LTT is in the expected temperature range. The diffraction data indicate that martensite formation is more rapid compared to the root due to lower segregation across the weld. LTT CrMn is characterized by low amounts of retained austenite at ambient temperature.

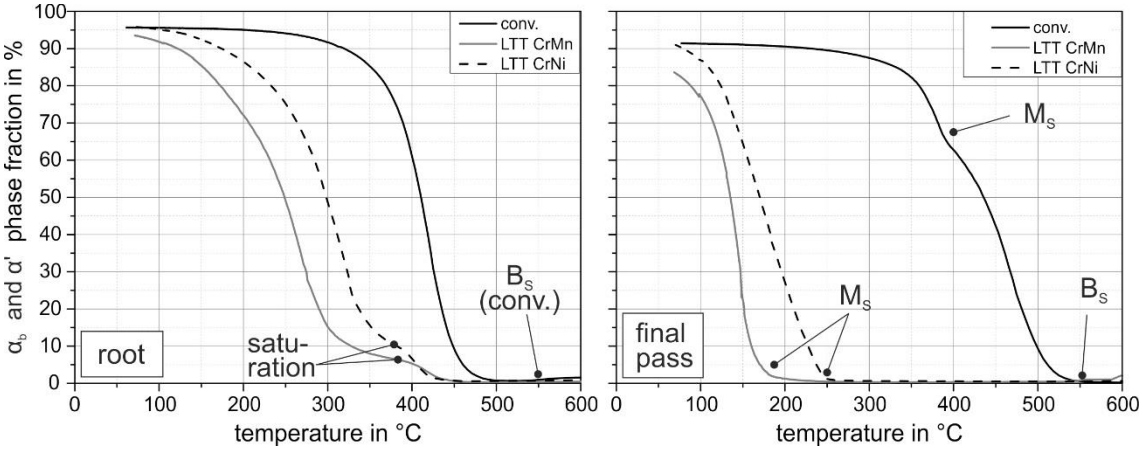

Figure 5: Development of the α_b and α' phase fraction during cooling after welding of the root pass (left, measuring depth = -8 mm) and after welding of the final pass (right, measuring depth = -2 mm)

Total strain during cooling

The total lattice strain was calculated after Equation (7) as a function of the phase specific lattice strains taking into account the amount of each phase fraction. Figure 6 shows the development of the total lattice strains vs. the temperature after welding of the root (left) as well as of the final pass (right) during cooling in longitudinal direction of the weld. In case of the root at high temperatures around 600 °C the lattice strain of

the conventional weld started in compression and was increased to around $\varepsilon_t = -1\times10^{-3}$ during cooling until M_s was reached. The phase transformation into bainite at 550 °C was not effective on the total lattice strain. After $M_s \approx 420$ °C the total lattice strain stayed approximately constant between $\varepsilon_t = 0$ and $\varepsilon_t = -1\times10^{-3}$. Obviously, the lattice strain induced by hindered shrinkage and the lattice strain induced by phase transformation had balanced each other until ambient temperature was reached.

Contrary to that high temperature tensile lattice strains up to $\varepsilon_t = 3\times10^{-3}$ were observed above M_s in case of the LTT weld metals in absence of bainite formation due to restrained shrinkage. The first martensite formation at about 420 °C (transition to HAZ) counteracts the shrinkage and kept the lattice strain at an almost constant level between $\varepsilon_t = 1\times10^{-3}$ and $\varepsilon_t = 3\times10^{-3}$. After M_s of both LTT weld metals were reached at about 360 °C for the LTT CrNi and about 327 °C for the LTT CrMn the lattice strains decreased from tension to compression with ongoing martensite formation. At ambient temperature compressive lattice strains comparable (respectively below for LTT CrMn) to the conventional weld are present. Despite different initial strain levels, the low-temperature martensitic transformation in the LTT welds ensures that comparable strain levels are present at ambient temperature.

Investigating the final pass (Fig. 6, right), the lattice strain formation of the conventional weld was qualitatively comparable to that of the root. Again, the influence of the bainite phase transformation on the lattice strain was negligible. Tensile lattice strain rised up to about $\varepsilon_t = 1.6\times10^{-3}$ due to restrained shrinkage. When reaching M_s of the weld, the total tensile lattice strain was slightly reduced to about $\varepsilon_t = 1.3\times10^{-3}$. During further cooling the lattice strain was balanced at around $\varepsilon_t = 1.1\times10^{-3}$ until ambient temperature was reached. In contrast to the root, the total lattice strain of the final pass is tensile for the conventional weld. In case of the LTT welds the lattice

strains of the final pass do not increase significantly during cooling. The lattice strains are balanced at almost constant levels. While LTT CrNi is in compression around $\Delta\varepsilon_t = -0.5\times10^{-3}$, LTT CrMn is in tension approximately at the same level as the conventional weld. Nevertheless, when M_s at about 185 °C was reached, the lattice strain was quickly pushed into compression by the newly formed martensite to $\varepsilon_t = -1.5\times10^{-3}$. This continued until ambient temperature. In the LTT CrNi weld the lattice strain is decreased after M_s was reached at about 248 °C exactly to the same level. Therefore, at ambient temperature the amount of compressive lattice strain is similar between the LTT welds at about $\varepsilon_t = -1.5\times10^{-3}$.

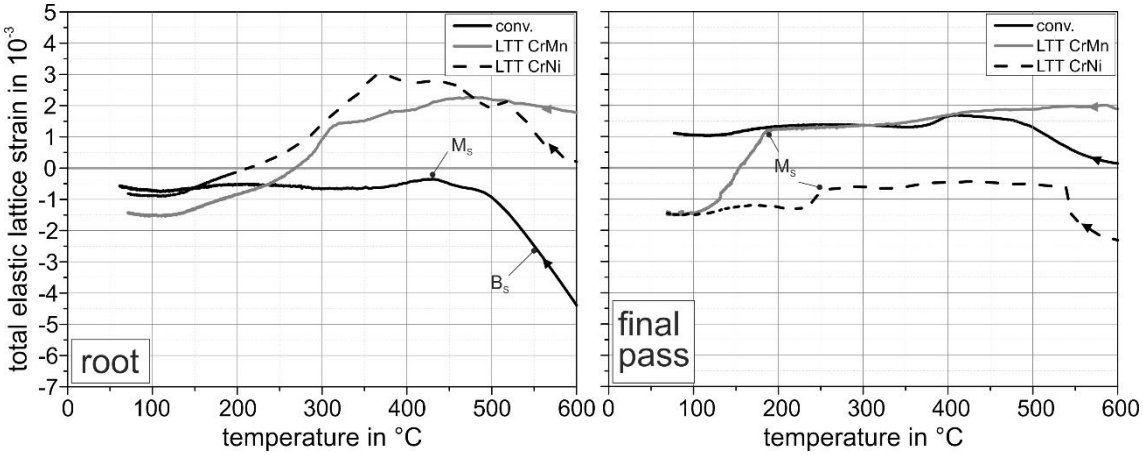

Figure 6: Total elastic lattice strain development of the LTT CrNi, LTT CrMn and conventional weld in longitudinal direction after welding of the root (left, measuring position at "-8 mm" in the root pass) and after welding of the final pass (right, measuring position "-2 mm" in the final pass)

While the difference of the total elastic lattice strain in the root after welding was only small between the filler materials investigated, the strain level of the final pass was much more influenced in case of the LTT filler materials. In contrast to the conventional weld compressive lattice strains were formed here. Despite this point the LTT CrNi behaved differently compared to LTT CrMn. To identify the differences between the

weld filler materials in detail, phase specific lattice strains of austenite and martensite are discussed separately in the following.

Phase specific lattice strain during cooling - root

Figure 7 shows the development of the phase specific lattice strain in longitudinal direction vs. temperature in the weld root determined during cooling for the γ (left) and α_b and α' phases (right) . It is important to notice that the development of the local phase specific lattice strains must be assessed with respect to the total strain (in terms of load partitioning) and thus in regard to the phase content. However, the level of strain in the austenite phase differs at about 600 °C. While the conventional weld is in compression the LTT welds are in tension. Due to restrained shrinkage in all cases the austenite lattice strain increased towards the tensile regime. The martensite phase transformation at about 420°C balanced the strain level or even decreased it somewhat in case of the conventional weld metal. Based on the diffraction data, the bainite phase transformation had no influence on the remaining lattice strain in the austenite phase. During further cooling the lattice strain in the austenite phase of the conventional weld kept growing and resulted in tensile lattice strains at ambient temperature. In contrast the lattice strains in the LTT welds were reduced when their specific M_s' were reached. The austenite phase of the LTT CrMn weld metal was larger affected. The lattice strain continuously decreased down to ambient temperature showing a compressive lattice strain of about $\varepsilon_\gamma = -1.5\times10^{-3}$. In contrast, the LTT CrNi weld metal and the conventional weld metal resulted both in tensile lattice strain of about $\varepsilon_\gamma = 2\times10^{-3}$.

In case of the α_b and α' lattice strain evolution remarkable compressive lattice strains were determined at a temperature of about 600 °C for all filler materials investigated. Nevertheless, the phase fraction of the α_b and α' phase was too low to influence the total lattice strain (Fig. 6) significantly. Note, that X-ray interference lines

for the α-phase were already measured above B_s. These very weak diffraction signals are assumed to stem from very small amounts of ferrite of the diluted weld or HAZ, which are not considered here. Furthermore, at this temperature the measurement error does not allow for an exact statement. During further cooling the compressive lattice strain decreases due to restrained shrinkage until M_s at about 420 °C. In the further course, the ongoing martensite formation in the weld with the conventional weld filler counteracted the shrinkage balancing the lattice strain at a constant level. At ambient temperature a lattice strain in the martensite phase of approximately $\varepsilon_{\alpha'} = -0.5\times10^{-3}$ was determined. For the LTT welds the martensite formed at about 420°C is limited to a small amount (7% - 10%, see Fig. 5). Due to dilution of the weld with the HAZ, M_s was increased and phase transformation began in the transition region of the weld to the HAZ. Therefore, high tensile lattice strains were determined in the austenite phase at the same time the lattice strain in the martensite phase abruptly rised into the tensile regime. Reaching the characteristic M_s of each LTT weld metal the phase specific lattice strains are continuously decreased until ambient temperature to a similar level as found for the conventional weld filler. The phase specific lattice strains in the root illustrate that the amount of martensite formed is crucial for counteracting shrinkage induced lattice strains. Too low amounts of martensite do not affect the lattice strain in the austenite phase. The data indicate, that the austenite phase is the dominant phase in regard to the total strain development.

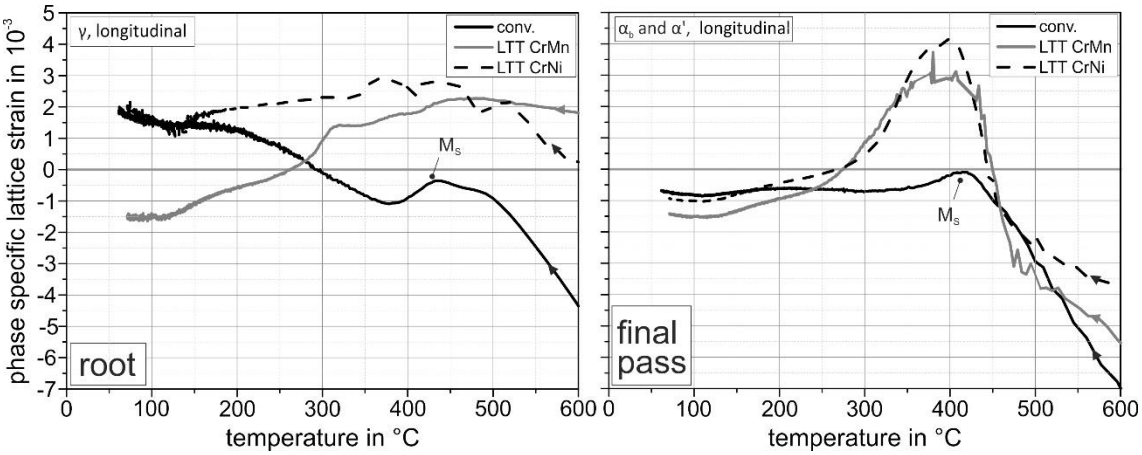

Figure 7: Phase specific lattice strain evolution vs. temperature in longitudinal direction of the γ phase (left) and the α_b and α' phase (right) during cooling of the root weld (z = -8 mm)

Phase specific strain during cooling – final pass

Figure 8 shows the development of the phase specific lattice strain vs. temperature in longitudinal direction for the γ (left) and α_b and α' phase (right) found during cooling of the final pass. Qualitatively, the lattice strain development in the conventional weld is similar to the courses discussed for the root pass. However, the strain level is shifted towards tensile values. This accounts for the austenite phase as well as for the martensite (and bainite) phases. The martensite formation barely affected the lattice strain in the austenite phase, which resulted in high tensile lattice strains above $\varepsilon_\gamma = 5\times10^{-3}$. For the martensite phase itself a nearly constant tensile lattice strain level during cooling to ambient temperature below a value of about $\varepsilon_{\alpha'} = 1\times10^{-3}$ was determined.

In contrast to the conventional weld filler the lattice strain in the austenite phase of the LTT welds was decreased when the specific M_s of the weld metals was reached. At ambient temperature compressive phase specific lattice strain was determined for the austenite phase with values of about $\varepsilon_\gamma = -2\times10^{-3}$. The lattice strain in the martensite phase of the LTT weld metals behaved differently from the root layer. For the LTT

martensite phase first α X-ray interference lines were determined in absence of any HAZ related martensite/bainite/ferrite-phase as found for the root. Therefore, the first lattice strain values determined for the martensite phase are highly compressive around $\varepsilon_{\alpha'} = -6.5\times10^{-3}$ independent from the LTT filler investigated. With increasing amount of martensite the lattice strain quickly raised up to about $\varepsilon_{\alpha'} = -1\times10^{-3}$. After 50% of martensite had formed the lattice strain stayed nearly constant at that level down to ambient temperature. Further increase of the martensite phase fraction due to ongoing martensite phase transformation counteracts the lattice strain development induced by shrinkage restraint. On the other hand, the temperature gradient decreases over the weld seam length (longitudinal) during cooling, hence, also the restrained thermal contraction of the weld seam decreases. As a result, phase transformation of the LTT welds will have a more positive effect on the strain state. The heat flux during cooling depends on physical factors as well as on the sample size. Thus, the limit value mentioned above (50% martensite) cannot be generalized.

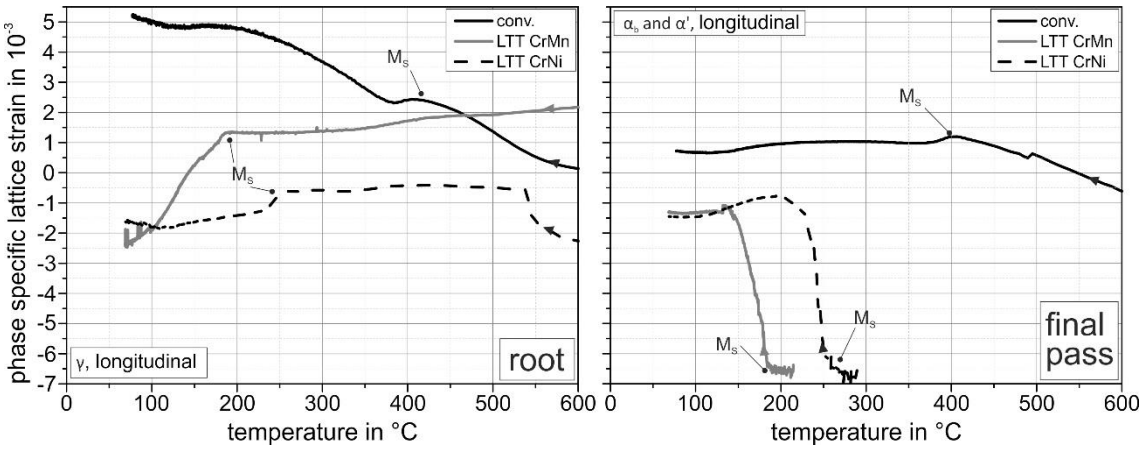

Figure 8: Phase specific lattice strain evolution vs. temperature in longitudinal direction of the γ phase (left) and the α_b and α' phase (right) during cooling of the final pass of the weld (z = -2 mm)

Similar to the root the characteristic martensite formation in the LTT welds of the final pass induced high compressive lattice strains. However, in case of the root pass

the lattice strain is an accumulated signal containing diluted areas of the HAZ (see Fig. 4) next to the pure weld metal. In consequence, the lattice strains found for the root pass somehow smear the "LTT effect". As one conclusion, the evaluation of the efficiency of LTT fillers should be based on the final pass.

In principle the theoretical model of stress formation during cooling of a weld metal undergoing phase transformation after Nitschke-Pagel and Wohlfahrt **[4]** was proven for a multi-pass weld in the present study. Even more an in-situ diffraction experiment allowing for a separation of the phase specific lattice strain in austenite and martensite was realized.

Using LTT filler materials the total elastic lattice strain of the weld was significantly reduced compared to the conventional weld filler but dilution must carefully be considered. Due to the lower M_s of the LTT filler materials, tensile lattice strain of the austenite phase was decreased to compression while for the conventional weld filler restrained shrinkage led to tensile lattice strains. In contrast to the conventional weld filler delayed and ongoing martensite phase transformation of the LTT weld led to compressive lattice strains for the martensite phase. Worth mentioning, also in the conventional weld the undergoing martensite formation could balance the shrinkage induced lattice strains in the martensite phase to about $\varepsilon_{\alpha'} = 0.85\times10^{-3}$**.**

Conclusions

In-situ diffraction analysis during GMA multi-pass welding was conducted to observe the effect of martensite formation on the phase specific lattice strains of the root pass as well as of the final pass, which developed during cooling and after deposition of each layer. In addition to the LTT CrNi concept, the strain evolution of a LTT CrMn alloy was investigated here. The results were compared to the lattice strain evolution of a

conventional weld filler material. From the results obtained, the following conclusions can be drawn:

- M_s varies in case of the LTT joints over the weld cross section due to dilution of the weld with the heat affected zone. For the sample used, this is most pronounced for the root pass as the contact area between weld metal and base material is larger. Depending on the amount of dilution also the content of the phase fractions was slightly altered.
- In contrast to the sample used in earlier studies **[19-21]** the total elastic lattice strain in longitudinal direction was reduced by delayed martensite formation using LTT filler materials despite a higher restraint intensity of the sample used here. The volume expansion due to the martensite phase transformation counteracted the lattice strains formed by restrained shrinkage. In case of the martensite phase of the final pass even higher compressive lattice strain was induced during welding for the LTT CrNi weld filler material in comparison to the sample used in previous studies **[20]**.
- The martensite phase transformation decreased the lattice strain in the austenite phase. While this effect is leading to compressive lattice strain in case of the LTT welds for the austenite phase of the conventional weld filler still tensile lattice strains during cooling were determined.
- High compressive lattice strains were present in the appearing martensite phase when M_s was reached. The lattice strains decreased quickly due to restrained shrinkage but stayed in compression at ambient temperature. For the sample used here, the reduction of the compressive lattice strain stopped at a phase fraction of approx. 50% of martensite.

- Both LTT fillers (M_s = 230 °C and M_s = 123 °C) used in this study show a similar lattice strain formation during cooling despite different transformation temperatures. However, due to the pronounced dilution with the base material M_s in the root weld is raised compared to these nominal values. In case of the root the phase specific lattice strains of the LTT CrMn weld filler were reduced compared to the LTT CrNi weld fillers. The results indicate that for an optimal use of the LTT effect in the root of multi-pass welds the alloying concept must be adapted taking care of the dilution. On the other hand, the lattice strains in the final pass are significantly affected by the LTT martensite formation.

Acknowledgements

Parts of this research were carried out at the storage-ring-based X-ray radiation source PETRA III at DESY. The authors would like to thank DESY for granting beamtime. Further, the authors would like to especially acknowledge the German Research Foundation (DFG) for funding parts of this work (KA 1807/4-1 | GI 376/4-1), Lincoln Electric Europe for provision of welding consumables as well as EWM AG for support.

References

[1] Karlsson L.: Thermal Stresses in Welding: Thermal Stresses I. Amsterdam (NLD): Elsevier Science Ltd; 1986: 299–389

[2] Bretz W, Hoffmeister H. Effect of hydrogen, restraint and welding conditions on weld metal cold cracking of HSLA steels in the IRC test. mater technol. 1987;58(3):142–147

[3] Heeschen J, Wohlfahrt H. Residual Stresses in Science and Technology: Assessment of the Influence of Shot Peening on the Fatigue Strength of Butt Welded Joints. Oberursel (GER): DGM Informationsgesellschaft Verlag; 1987:467-476

[4] Nitschke-Pagel T, Wohlfahrt H. Residual Stresses in Welded Joints - Sources and Consequences. mater sci forum. 2002;404-407:215-226

[5] Jones W K C, Alberry P J. Residual stresses in welded construction and their effects: A model for stress accumulation in steel during welding. British Weld Res Association; 1978:15–26

[6] Ohta A, Watanabe A, Matsuoka K, et al. fatigue strength improvement by using newly developed low transformation temperature welding material. weld world. 1999;43(6):38-42
[7] Wang W,Huo L, Zhang Y, et al. New Developed Welding Electrode for Improving the Fatigue Strength of Welded Joints. J mater sci & technol. 2002;18(6):527–531
[8] Kromm A, Dixneit J, Kannengiesser T. Residual stress engineering by low transformation temperature alloys-state of the art and recent developments. Weld world. 2014;58(5):729-741
[9] Bhadeshia H K D H, Street P, Cb C. Developments in Martensitic and Bainitic Steels : Role of The Shape Deformation Materials Science and Metallurgy. mater sci & eng A. 2004;A378:34–39
[10] Dai H, Francis J A, Stone H J, et al. Characterizing phase transformations and their effect on ferritic weld residual stresses with X-rays and neutrons. metall mater trans A. 2008;39:3070–3078
[11] Shiga C, Yasuda H Y, Hiraoka K, et al. Effect of M_s temperature on residual stress in welded joints of high-strength steels. Weld World. 2010;54:71–79
[12] Kromm A, Kannengiesser T, Altenkirch J, et al. Residual Stresses in Multilayer Welds with Different Martensitic Transformation Temperatures Analyzed by High-Energy Synchrotron Diffraction. mater sci forum. 2011;681:37-42.
[13] Ramjaun T, Stone H J, Karlsson L, et al. Effect of interpass temperature on residual stresses in multipass welds produced using low transformation temperature filler alloy. sci technol weld join. 2014;19(1):44-51
[14] Dixneit J, Kromm A, Boin M, et al. Influence of Heat Control on Residual Stresses in Low Transformation Temperature (LTT) Large Scale Welds. mater res proc (ICRS-10). 2016;2:223–228.
[15] Kromm A.: Evaluation of weld filler alloying concepts for residual stress engineering by means of Neutron and X-ray diffraction. adv mater res. 2014;996:469-474
[16] Gibmeier J, Obelode E, Altenkirch J, et al. Residual stress in steel fusion welds joined using low transformation temperature (LTT) filler material. mater sci forum. 2014;768-769:620-627
[17] Kromm A, Kannengiesser T. Effect of martensitic phase transformation on stress build-up during multilayer welding. mater sci forum. 2014;768-769:660-667
[18] Altenkirch J, Gibmeier J, Kromm A, et al. In situ study of structural integrity of low transformation temperature (LTT)-welds. mat sci & eng A. 2011;528(16-17):5566-5575
[19] Altenkirch J, Gibmeier J, Kostov V, et al. Time- and temperature-resolved synchrotron X-ray diffraction: observation of phase transformation and strain evolution in novel low temperature transformation weld filler materials. The J of Strain Analysis for eng des. 2011;46(7):563–579
[20] Gibmeier J, Held E, Altenkirch J, et al. Real time monitoring of phase transformation and strain evolution in LTT weld filler material using EDXRD. J of mater process technol. 2014;214(11):2739–2747
[21] Kromm A, Kannengiesser T, Gibmeier J: In-Situ Observation of Phase Transformations during Welidng of Low Transformation Temperature Filler Material. mater sci forum. 2010;638-642:3769-3774
[22] Vollert F; Dixneit J, Gibmeier J, et al. In Situ EDXRD Study of MAG-Welding Using LTT Weld Filler Materials under Structural Restraint. mater sci forum. 2017;905:107-113

[23] Satoh K, Ueda Y, Matsui S, et al. Japanese studies on structural restraint severity in relatio to weld cracking (Preliminary report). weld world. 1977;15(7/8):155–162
[24] Kromm A, Rhode M, Kannengiesser T: Influence of heat control on welding residual stresses in multi-layer component joints. In: Babu S, Bhadeshia H K D H, Cross C E, et al., editors. Trends in welding research - Proceedings of the 9th international conference; 2013; Chicago (IL, USA), p. 48-54
[25] Francis J A, Smith M C, Jeyaganesh B, et al. Design and Manufacture of Industrially Representative Weld Mock-ups for the Quantification of Residual Stresses in a Nuclear Pressure Vessel Steel. mater res proc (ICRS-10). 2016;2:581–586
[26] Dai H, Moat R J, Withers P J: Modelling the interpass temperature effect on residual stress in low transformation temperature stainless steel welds. In: ASME PRESSURE VESSELS AND PIPING CONFERENCE. 2011;6(Part B):1451–1458). Baltimore (MD, USA).
[27] Gadallah R, Murakawa H. Numerical Study on Influence of Specimen Size upon Welding Residual Stress. In: Visual-JW The International Symposium on Visualization in Joining & Welding Science through Advanced Measurements and Simulation; 2014; Osaka (JPN) p. 324–325
[28] Schell N, King A, Beckmann F, et al. The High Energy Materials Science Beamline (HEMS) at PETRA III. mater sci forum. 2013;772:57–61
[29] Schwenk C, Kannengiesser T, Rethmeier M: Restraint Conditions and Welding Residual Stresses in Self-Restrained Cold Cracking Tests. In: Trends in Welding Research, Proceedings of the 8th International Conference; 2008 June 1-6; Callaway Gardens Resort, Pine Mountain (GA, USA)
[30] Weidemann J, Dixneit J, Kromm A, et al. INFLUENCE OF STRUCTURAL STIFFNESS ON THE RESIDUAL STRESSES DURING WELDING OF LOW TRANSFORMATION TEMPERATURE ALLOYS. In: Sommitsch C, Enzinger N, Mayr, P. editors. Mathematical Modelling of Weld Phenomena 11. Proceedings of the 11th International Seminar Numerical Analysis of Weldability. 2015; Seggau (AUT) 2016. p. 259–276
[31] International Organization for Standardization. Welding consumables - Wire electrodes, wires, rods and deposits for gas shielded arc welding of high strength steels – Classification. 2012. Standard No. DIN EN ISO 16834
[32] European Standardization. Hot rolled products of structural steel – Part 6: Technical delivery conditions for flat products of yield strength structural steels in the quenched and tempered condition. 2004. Standard No. DIN EN 10025-6
[33] Hammersley A P. FIT2D: An Introduction and Overview. 1997. (*ESRF Internal Report*, ESRF97HA02T)
[34] Hammersley A P, Svensson S O, Hanfland M, et al. Two-Dimensional Detector Software: From Real Detector to Idealised Image or Two-Theta Scan. High press res. 1996;14:235-248
[35] Laine E S U: A high-speed determination of the volume fraction of ferrite in austenitic stainless steel by EDXRD. J of Physics F: Metal Physics, 1978;8(7):1343–1348
[36] Darken L S; Smith R P. Thermodynamic Functions of Iron. ind and eng chem. 1951;43(8):1815–1820
[37] Chantler C T: Theoretical Form Factor, Attenuation, and Scattering Tabulation for Z=1–92 from E = 1–10 eV to E = 0.4–1.0 MeV. J. physics. chem. ref. data. 1995;24(1):71–643

[38] Chantler C T, Olsen K, Dragoset R A; et al. X-Ray Form Factor, Attenuation, and Scattering Tables. NIST database. 2001
[39] Daymond M R: The determination of a continuum mechanics equivalent elastic strain from the analysis of multiple diffraction peaks. J of appl physics. 2004;96(8):4263–4272
[40] Macherauch E; Zoch H-W: Praktikum in Werkstoffkunde 91 ausführliche Versuche aus wichtigen Gebieten der Werkstofftechnik [practical training in material science 91 experiments from the most important fields of material science]. Wiesaden (DEU): Vieweg+Teubner Verlag; 2011. p. 114. in german
[41] Spieß L, Teichert G, Schwarzer R, et al. Moderne Röntgenbeugung. Röntgendiffraktormetrie für Materialwissenschaftler, Physiker und Chemiker [modern x-ray diffraction. x-ray diffraction for material scientists, physicists and chemists]. Wiesbaden (DEU): Vieweg+Teubner Verlag; 2009, p. 241. in german
[42] Held E, Ohl H, Gibmeier J, et al. Mikrostruktur- und Härteentwicklung in Schweißnähten mit neuartigen LTT-Schweißzusatzwerkstoffen [Microstructure and hardness development in welds using new LTT weldding consumables] In: Lohrmann M, Rettenmayr M, editors. 45. Sonderband der Praktischen Metallographie. Fortschritte in der Metallographie - Proceedings der 47. Metallographie-Tagung; 2013; Friedrichshafen (DEU), p. 297-302. in german
[43] Kromm A, Kannengiesser T, Gibmeier J, et al. DETERMINATION OF RESIDUAL STRESSES IN LOW TRANSFORAMTION TEMPERATURE (LTT -) WELD METALS USING X-RAY AND HIGH ENERGY SYNCHROTRON RADATION. weld world. 2009;53(1/2):3–16
[44] Kromm A: Umwandlungsverhalten und Eigenspannungen beim Schweißen neuartiger LTT-Zusatzwerkstoffe [phase transformation behaviour and residual stresses during welding of new LTT filler materials]. Berlin (DEU): BAM Bundesanstalt für Materialforschung und –prüfung; 2011, p. 87. in german
[45] Steven W, Haynes A G. The temperature of formation of martensite and bainite in low-alloy steels. J Iron Steel Inst. 1956;183(8):349–359

Figure 1

Click here to access/download;Colour figure;Bild_1v3.jpg

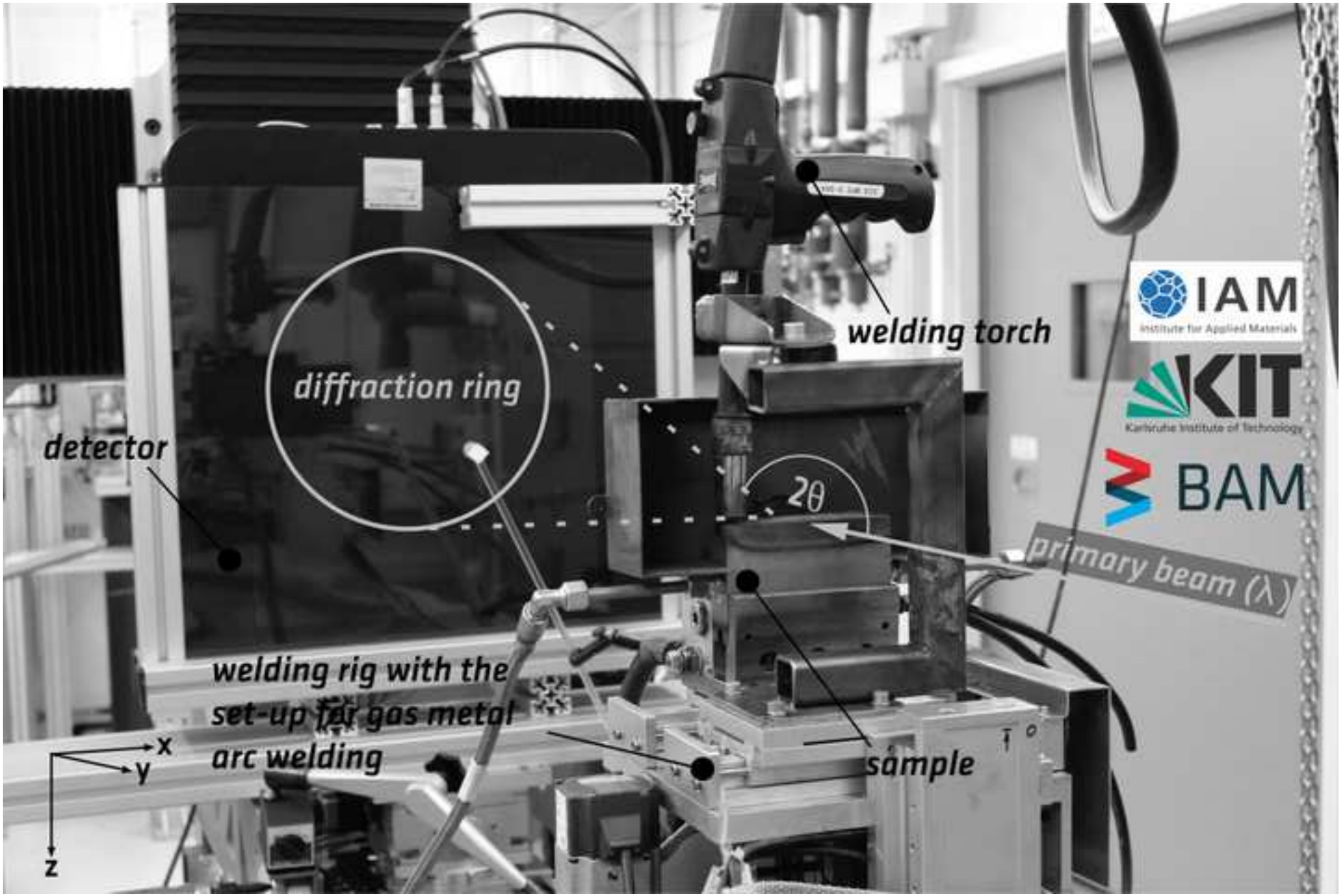

Figure 2

Click here to access/download;Colour figure;Bild_2v2.jpg

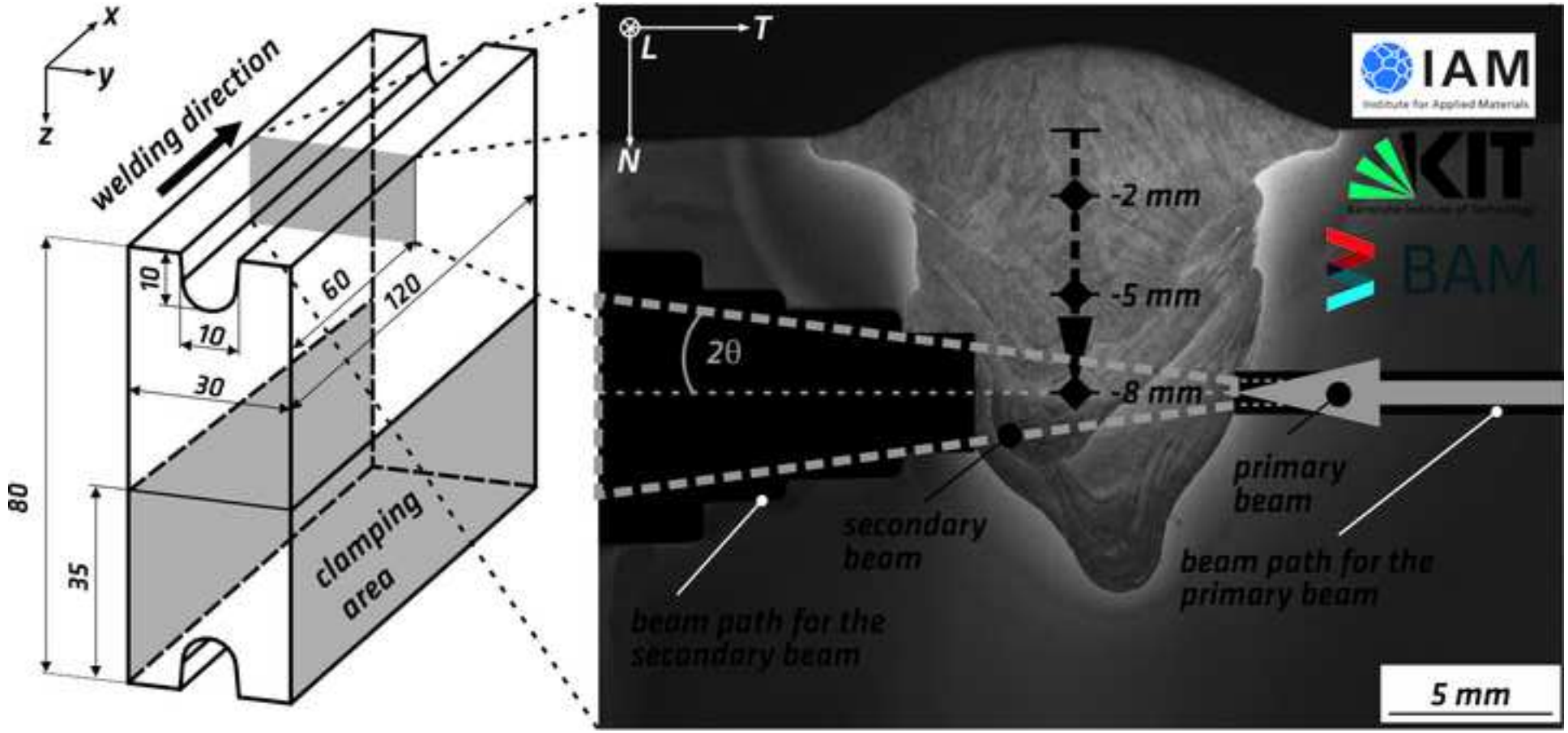

Figure 3

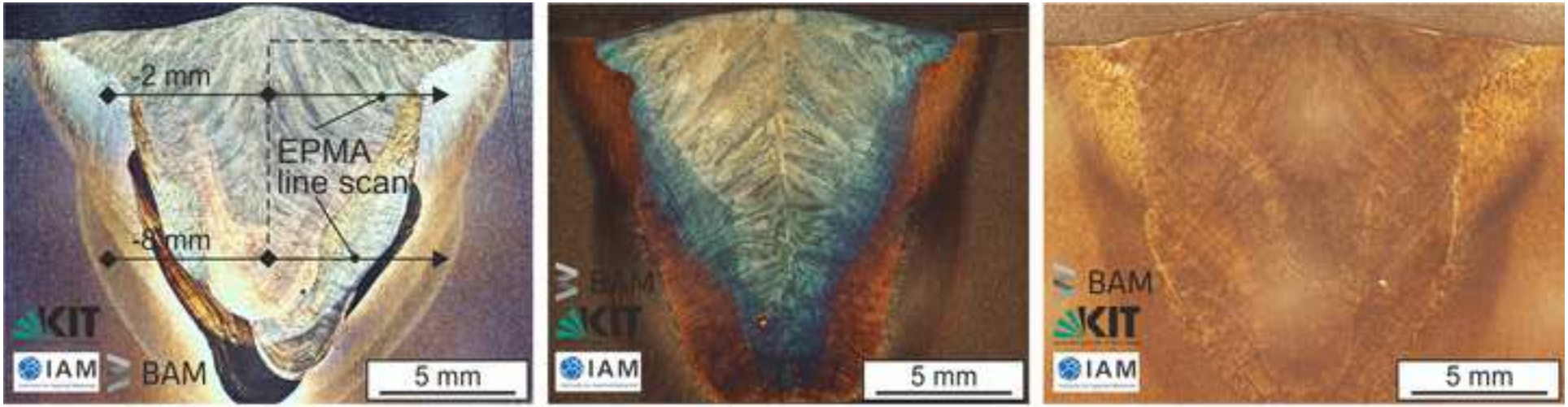

(a) weld „LTT CrMn“ (b) weld „LTT CrNi“ (c) weld „conventional“

Figure 4

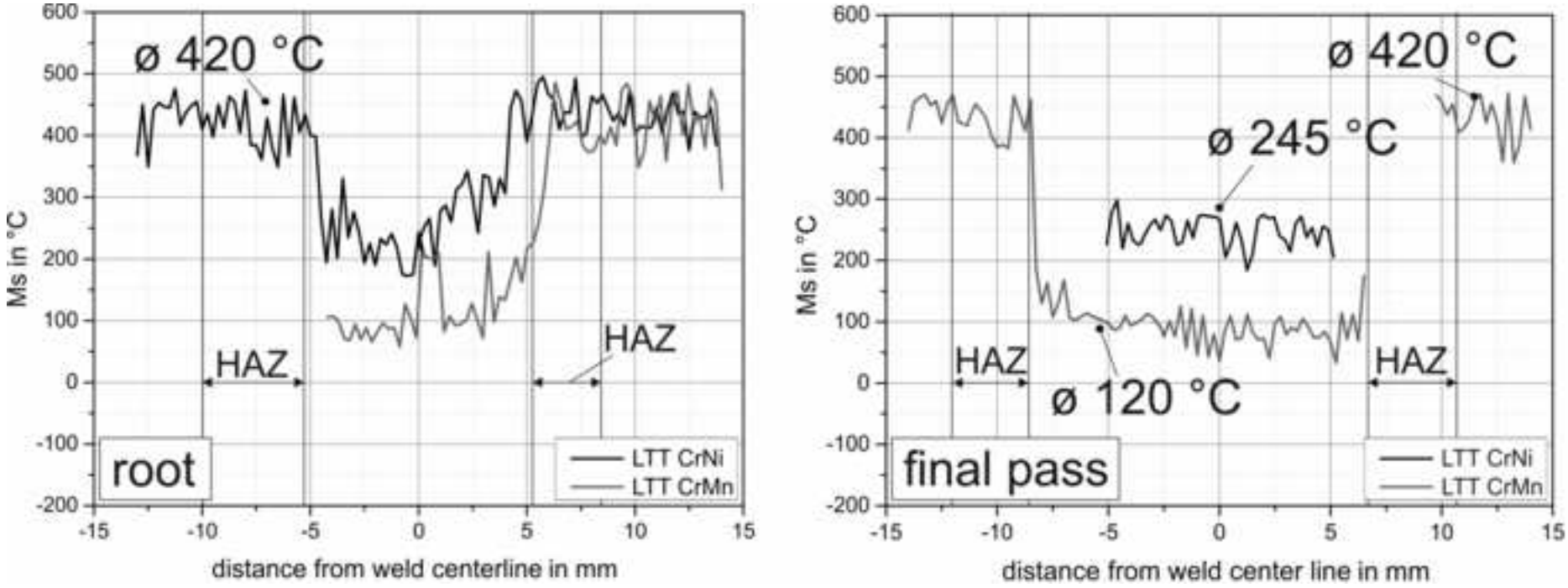

Figure 5

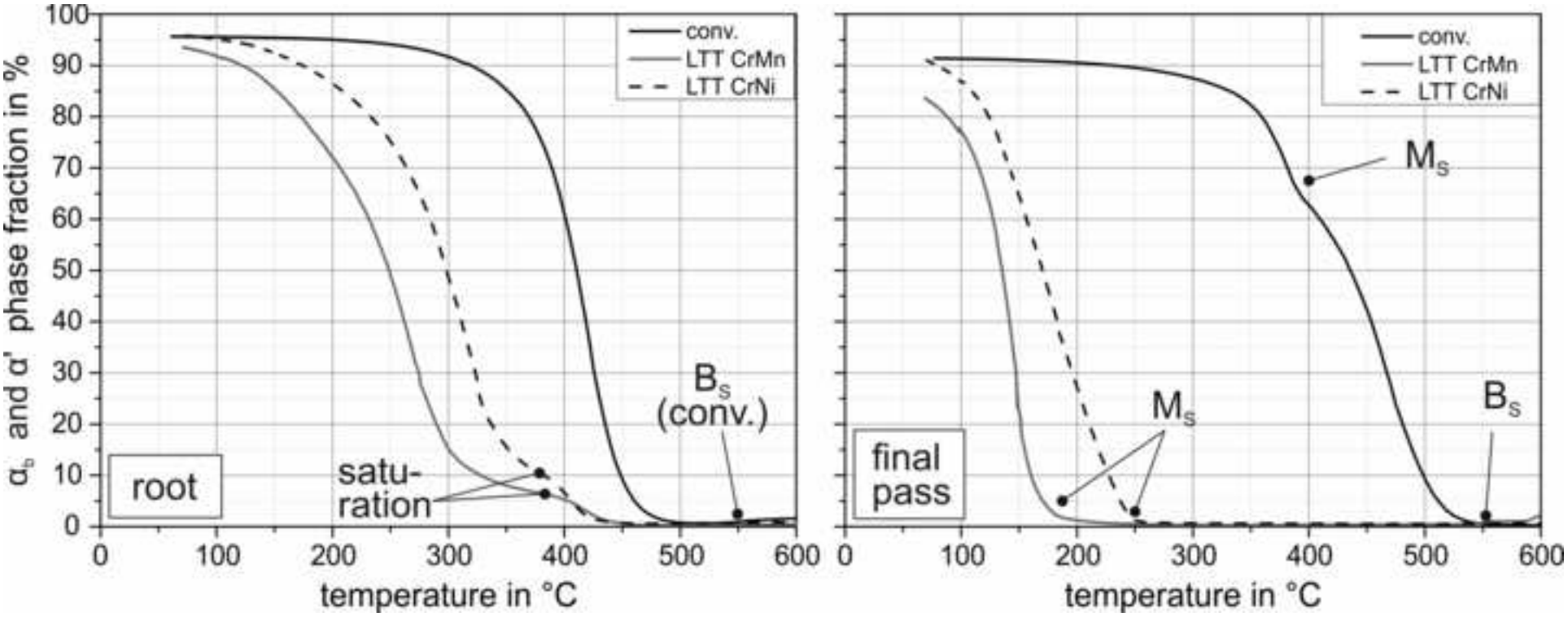

Figure 6

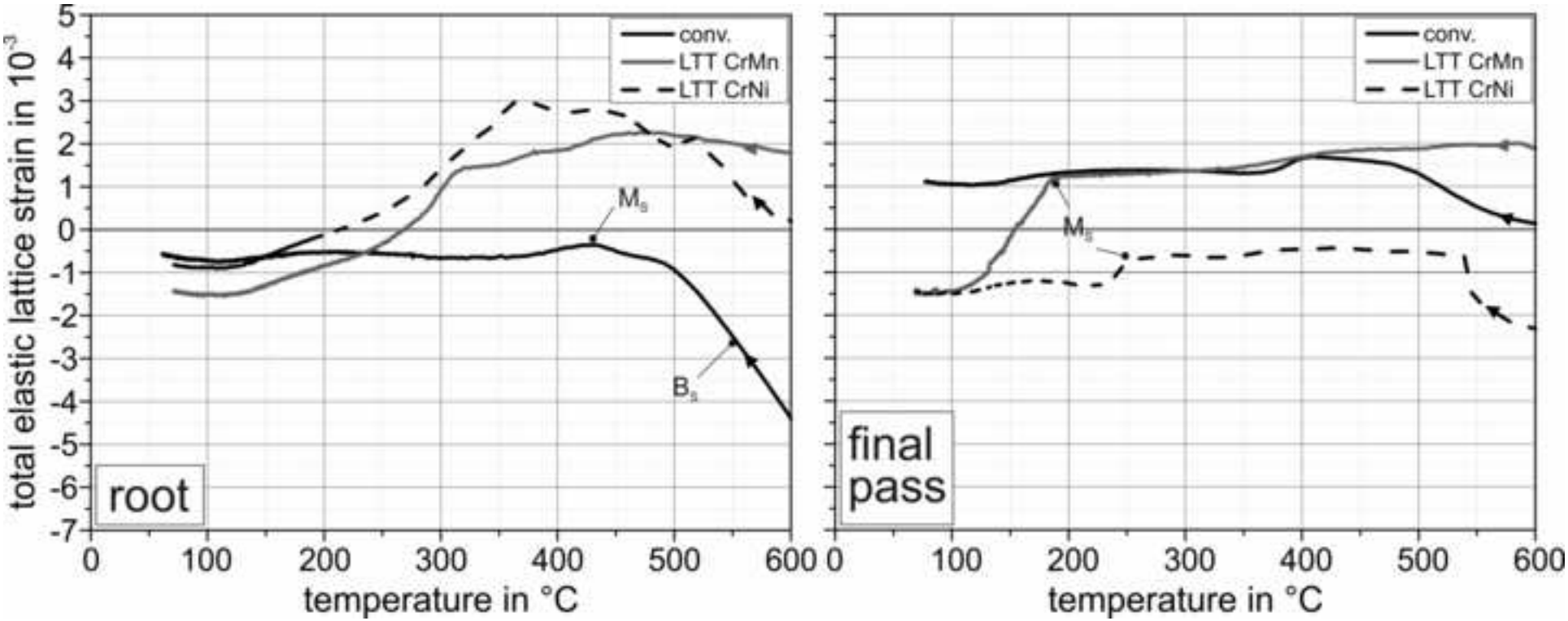

Figure 7

Click here to access/download;Non-colour figure;Bild_7nv1.jpg

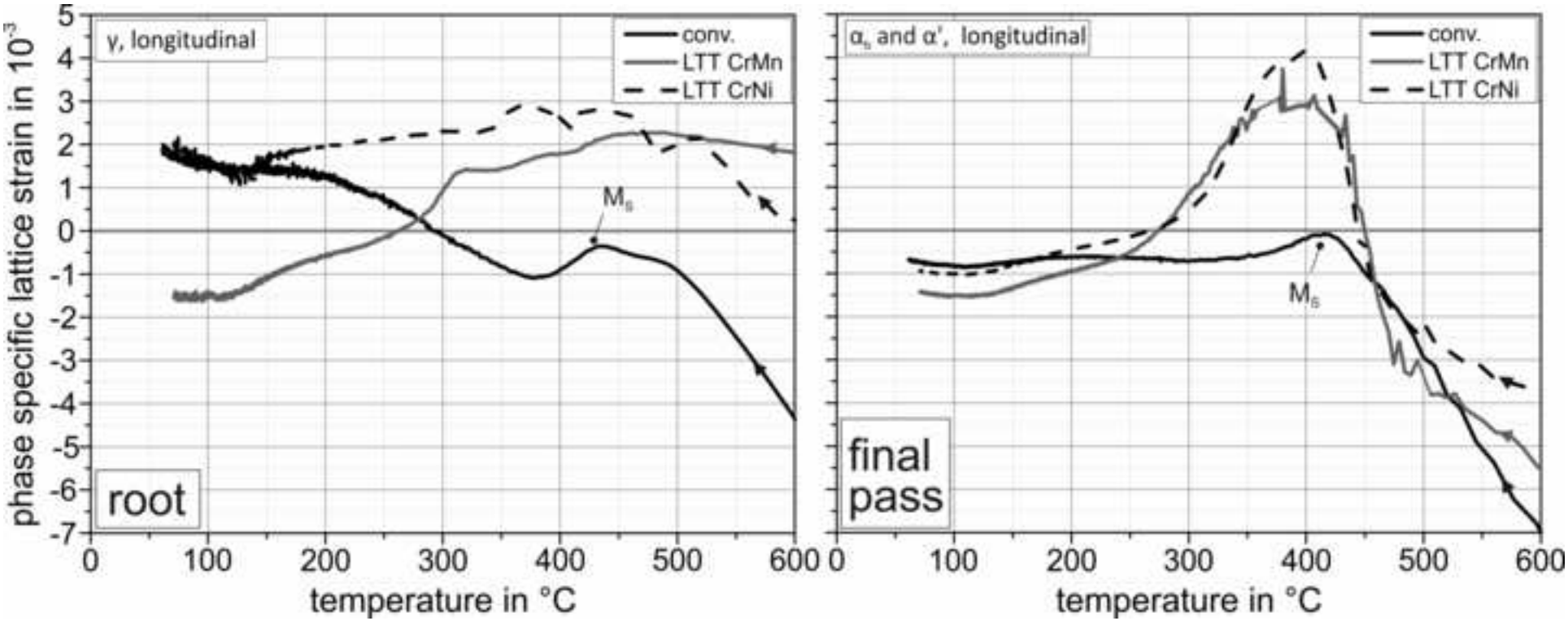

Figure 8

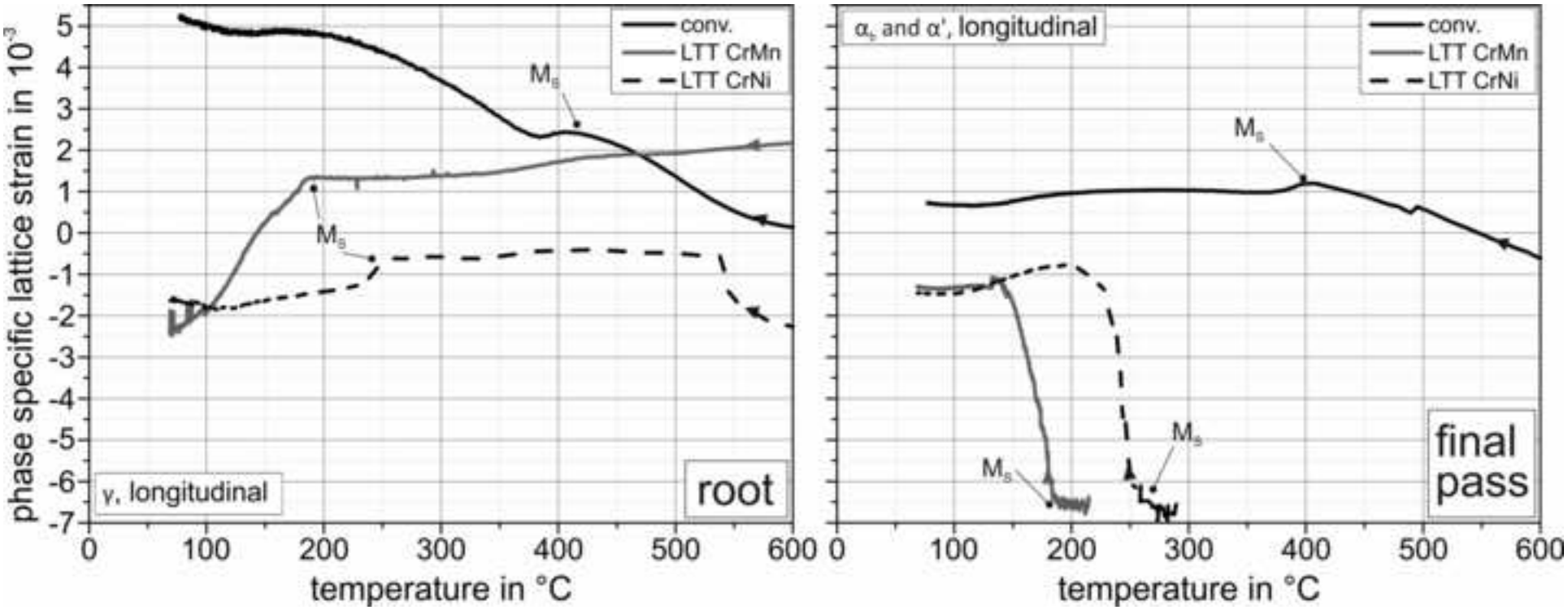

Ref.: STW4710
real time assessment of the strain evolution during GMA welding of low transformation temperature filler materials (LTT)

Reviewers' comments (Reviewer #1):

I reviewed the article by Dixneit et al. in which the authors have clearly described the outcome of some in-situ measurements of strain evolution during arc welding, using synchrotron X-ray diffraction method. The experimental setup is "smart" and the results are well presented.

However, the experimental method is already covered in the authors' previous publications (rightfully acknowledged in this submission too - Ref 19&20). Regarding the reported results, I checked all 6 bulleted conclusions and hardly found any new understating of such a well-researched field. For instance, the stress mitigating effect of LTT weld alloys, presence of compressive stresses in LTT weldments (vs. tensile in nontransforming weld alloys), the adverse effect of dilution in shifting up the Ms temperature and compromising the stress-mitigatigating performance of LTT alloys, all are published and well-known facts.

Hence, I am sorry that I am unable to recommend the submission for publication in STWJ.

Author comment:

We appreciate Reviewer #1 advice and help to improve the quality of the work. We hope this new revised version will comply with the high journal standards. Thank you for the review.

We have reviewed our conclusions in conjunction with our previous publications. We are now convinced that we have better highlighted the novelty value.

For instance Ref. 19 /20 are dealing with the re-melting of the pure LTT CrNi weld under free shrinkage. Strain measurements were performed at the surface and in the volume of the weld. In our opinion, a transferability of the previous results to multi-pass welding cannot be assumed without experimental verification. This is the topic of the present paper. In addition the new sample used here exhibit a high intensity of restraint comparable to real-life like multi-pass welds. The idea of the paper is to introduce in-situ strain analyses under more realistic (multi-pass) welding conditions. The strains we have determined show the difference between re-melting and multi-pass welding.

As a first step, in the present paper we focused on root welding to understand the influence of segregation on the strain development in this layer. Therefore we used EPMA analyses not only for the LTT CrNi but also for the new alternative LTT concept LTT CrMn to assess the Ms distribution over the welds cross section, which was not done so far. In connection with our literature research on LTT consumables, there are currently no publications that show experimentally and quantitatively the influence of segregation on the strain level of the root layer during cooling. The total elastic strain analyses of the root pass revealed, that the influence of dilution is different between the LTT alloys used. The LTT CrMn exhibit lower strain values compared to the LTT CrNi. Therefore the buildup sequence of the weld need to be adapted on the expected load level of the component. In a second step, we deal with the phase specific strain evolution during cooling of the final pass, in which the influence of segregation is reduced, right. This was not done for the LTT CrMn weld so far and was necessary as a reference to the root and for further planned publications dealing with repair welding or different heat input / heat fluxes.

In the previous studies differences were found for M_S of the LTT CrNi weld due to different procedures used (thermo cam, backward calculation from strain data) but an evaluation was not executed. In conjunction with Ref. 30 we did more precise temperature measurements and FE simulation to assess the heat flux of the sample. Furthermore EPMA analyses revealed, that the Ms distribution need to be

clearly understood to assess the strain evolution, which is not quantitatively published so far for different LTT alloys and multi-pass welds in conjunction with strain analyses.

With kind regards

Jonny Dixneit

R~~r~~eal time assessment of the strain evolution during welding using low transformation temperature filler materials

Jonny Dixneit[1], Florian Vollert[2], Arne Kromm[1], Jens Gibmeier[2], Andreas Hannemann[1], Thomas Kannengiesser[1]

[1]*Bundesanstalt für Materialforschung und -prüfung (BAM), Unter den Eichen 87, 12205 Berlin, Germany*

[2]*Karlsruhe Institute of Technology (KIT), Engelbert-Arnold-Straße 4, 76131 Karlsruhe, Germany*

Jonny Dixneit, jonny.dixneit@bam.de

~~real~~ Real time assessment of the strain evolution during welding using low transformation temperature filler materials

For the first time, local phase transformation kinetics and the strain evolution of the weld during gas metal arc welding were investigated and compared between novel low transformation temperature filler materials and a conventional welding consumable. Time-resolved diffraction analysis during welding was carried out. Compared to a conventional weld the total strain was reduced and compression strain was achieved when using LTT filler materials. During martensite phase transformation the austenite in the LTT welds was forced into compression strain longitudinal to the weld. Also, the martensite phase was in compression. This was most pronounced for the final weld pass. The strain evolution in the root pass was sensitive to increased phase transformation temperatures due to dilution with the base material.

Keywords: Low transformation temperature filler materials; Dilution; Phase transformation; Multi-pass welding; GMAW; Strain; Synchrotron diffraction; ADXRD

Introduction

Increasing demands on the integrity of welded components led to special focus on base material selection and material-specific design, e.g. in steel industry. Using high-strength steels *(HSS)* wall thicknesses are reduced as well as remarkable weight savings and lower processing costs are achievable. Unfortunately, HSS are sensitive to residual stresses due to their limited ductility. The residual stress condition of a welded structure depends on thermal, metallurgical as well as mechanical factors **[1]**. The combination of high hardness, low ductility and tensile residual stresses makes the welded joint susceptible to cold cracking **[2]** while life time expectancy appears unimproved under certain circumstances **[3]**.

Stresses during welding and subsequent cooling are induced due to the localized heat input. Based on this the resulting residual stress state is affected by the interaction

of local hindered shrinkage (restraint) of the weld and the heat affected zone *(HAZ)* as well as due to phase transformations. First concepts about the formation of welding residual stress were based on simple qualitative linear superposition of those factors. For example, basic principles of the impact of weld phase transformations on the stress development were already discussed by Nitschke-Pagel and Wohlfahrt **[4]**. Following this approach, during cooling the yield strength of the austenite phase limits the formation of high shrinkage induced tensile stresses at this stage. As phase transformation of the weld starts compressive stresses are induced due to hindered volume expansion. The amount of compressive stresses increases with decreasing phase transformation temperature as the yield strength of martensite increases too. After the phase transformation has finished tensile stresses may develop again due hindered shrinkage of the weld during cooling to ambient temperature. This was already proven by a well-known experiment of Jones and Alberry **[5]**, where simple heating trials of different materials have shown different levels of stress depending on the phase transformation temperatures. Nevertheless, these simple models do not allow to predict or to interpret the phase specific residual stress formation in complex multi-pass welds. This becomes important when dealing with residual stress engineering in welding.

Beside the application of post-weld treatments specific control of the welding stresses by means of martensite phase transformation becomes a practical meaning by so called Low Transformation Temperature (*LTT*) filler materials **[6-8]**. LTT alloys are a smart approach of an in-situ control of the stress development during fusion welding. The idea is to reduce tensile residual stresses or even to induce compressive ones already during the welding cycle by delayed martensitic phase transformation which compensates for thermal stresses **[9]**. Therefore, these alloys exhibit considerable reduced martensite-start-temperatures (M_s) and high yield strengths through tailored

chemical compositions. This allows to control the stress development in welded joints as already shown for small scale samples **[10-12]**. Specific research on LTT alloys with adapted M_S revealed that the existence of compressive residual stresses due to LTT is not to be generalized. The boundary conditions have significant effects on the level and distribution of residual stresses in welded joints, too. Beside the type of weld (i.e. butt weld, fillet weld) the heat input is most important **[13, 14]**. Moreover, differences occur between longitudinal and transverse residual stress distributions as well as between the surface and the bulk of the weld **[15, 16]**. In some cases even unexpected high tensile stress values were observed **[17]**.

Also, the microstructure can alter the residual stresses. As certain amounts of austenite are likely to remain due to unfinished martensite formation, stresses in both phases are to be considered **[18]**. Residual stress measurements using diffraction or semi-destructive methods (i.e. contour method or incremental hole drilling) allow for accurate evaluation of the residual stresses in LTT welded joints. But these ex-situ techniques do not provide an insight into the mechanisms of stress formation during welding and subsequent cooling. In-situ techniques are required for this. In particular diffraction techniques are predestinated here as they exclusively permit non-destructive spatial resolved access to the microstructural features as a function of time and temperature. As a result any phase transformation and mechanical as well as thermal strains can be observed.

Commented [A1]: The word “this” is unclear!

Commented [A2R1]: Done

Commented [A3]: Interesting choice of word. Not exactly appropriate. Suggest change!

Commented [A4R3]: done

In-situ diffraction studies dealing with the phase transformation kinetics of LTT filler materials have been already reported by the authors **[19, 20]**. After first investigations including simple heating and cooling of LTT alloys, welding (re-melting) was realized by Gas Tungsten Arc Welding *(GTAW)* using a special sample geometry at different beamlines featuring varying experimental conditions (Fig. 1).

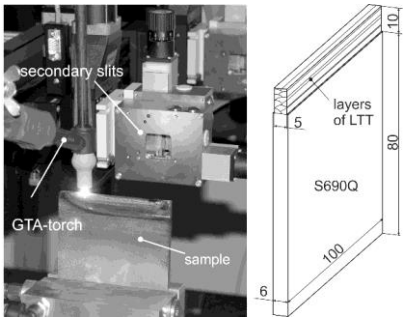

Figure 1: ~~test~~ Test set-up for in-situ diffraction studies during re-melting of welds (left) and sample geometry used to assess the phase transformation behavior and strain evolution in LTT-alloys (right), after [19-21]

Commented [A5]: Figure was removed due to word limit of the journal

As a result, phase transformation kinetics as well as strain development were directly observable during the re-melting process. It was concluded, that during cooling the austenite exhibits tensile strain longitudinal as well as normal to the welding direction. This is most pronounced in the bulk of the weld. In contrast to this, the martensitic phase shows compressive strain longitudinal to the welding direction while in normal direction tensile strain was observed. Varying heat conduction may be responsible for different strains in both directions. The results show the necessity of time and spatial resolved measurements. Ideally, the time resolution reflects the temperature gradient. The experiments reported up to now just simplified the welding process. In extension, welding specific features such as varying thermal cycles caused by multi-pass welding as well as realistic restraint conditions must be included to reproduce the stress-strain formation properly. Especially the restraint intensity, which represents a measure for the hindered shrinkage of the weld due to the stiffness of the joint surrounding, affects the residual stress formation considerably **[22-24].**

The latest publications about LTT alloys deal with the effect of the interpass temperature on the residual stresses in multi-pass welding **[14, 25-26]**. In the current work

the phase and strain formation during multi-pass welding under realistic restraint was observed in situ by Synchrotron diffraction.

Experimental

Time as well as spatial resolved angle dispersive synchrotron X-ray diffraction measurements during GMAW were performed at the High Energy Material Science beamline *(HEMS)* PETRA III P07 at DESY, Hamburg (Germany) **[27]** for the first time, see Figure 2. The sample was positioned perpendicular to the primary beam. Diffraction signals were measured using a digital X-ray flat panel detector (Perkin Elmer XRD1621). Measuring parameters are listed in Table **1**.

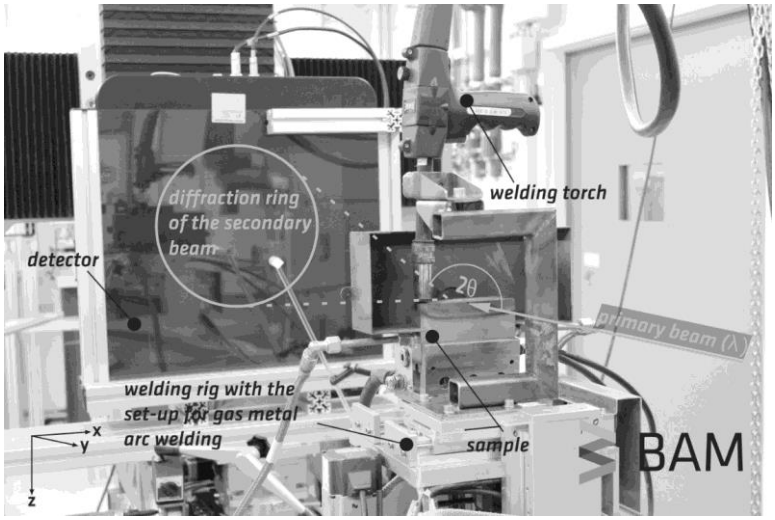

Figure 2: ~~test~~ Test set-up for in-situ diffraction studies using synchrotron x-rays during multi-pass welding (GMAW) @DESY PETRA III (P07), beam path shown schematically (gray)

To realize GMAW directly at the beam line a mobile and compact welding rig was designed. The setup has two parallel translation axes, carrying a GMAW torch and the weld sample mounted on one axis each. A third axis perpendicular allows the vertical adjustment of the whole set-up. The welding rig offers an accuracy of 100 µm achieved

Commented [A6]: Would prefer spelling out rather than abbreviation here.

Commented [A7R6]: ok

Commented [A8]: Should start figure caption with upper case.

Commented [A9]: Wow! 100 micron accuracy for torch carrying. Impressive! How much does this accuracy will affect actual welding and measurements?

Commented [A10R9]: The accuracy was necessary for alignment of the test rig in z to guarantee a free beam path through the holes of the sample. In addition the hexapod below the rig was also able to handle that. But this not always given at different beamlines. During welding this accuracy isn't entirely necessary for GMAW due to the huge weld pool

by using computer numerically controlled *(CNC)* servo-motors. All positioning and welding procedures take place by remote control as the experiments must be executed in a safety hutch.

Table 1: Measuring parameters of the angle dispersive x-ray diffraction experiment (AXRD)

Primary beam cross-section	1 × 1 mm²
Energy / Wave length primary beam	100 keV / 0.012398 nm
Measuring mode	transmission
Measuring frequency	2 Hz (during welding) / 0,5 Hz (during cooling down)
2θ	0 – 15°
Lattice planes	austenite: {200}, {220}, {311}; martensite: {200}, {211}, {220};
temperature at measuring stop	70 °C

sample geometry

Fusion bead-on-plate welding was performed using a special sample geometry with a high intensity of restraint transverse to the weld direction. As the working area at the beam line is limited but a high intensity of restraint would require large sample dimensions, a special sample geometry was designed, see Figure 3 (left). A solid block with a U-shaped gap was used to ensure a high stiffness of the weld surrounding. The dimensions of the gap made it possible to realize three passes between the fillets. Those fillets with a width of 10 mm act as a support plate while they were reinforced by the solid block below the weld to ensure a high intensity of restraint as known from large scale samples or specific weld tests **[28]**. The intensity of restraint of this U-shaped sample was already calculated by numerical simulation from R_{Fy} = 40 kN × mm^{-1} × mm^{-1} to $R_{Fy, total}$ = 65 kN × mm^{-1} × mm^{-1} depending on each welded pass. **[29]**.

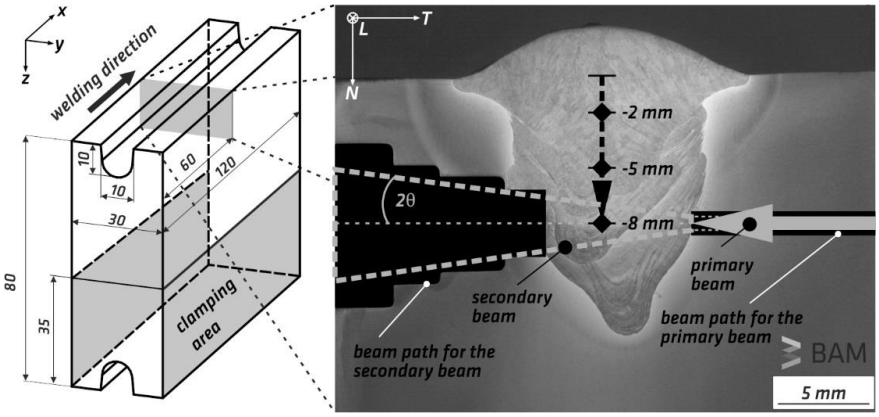

Fig. 3: isometric view of the sample in millimeter before welding (left) and cross section of the gauge area after GMA welding of the final pass (third layer), e.g. measuring position in a depth of -8 mm (right)

In order to obtain the diffraction information from the weld metal exclusively, drill holes for the primary and secondary beam paths were made horizontally into the fillets (Fig. 3 right). Loss of intensity due to attenuation effects could be kept to a minimum this way. On the secondary side the hole-diameter was increased stepwise in order to account for the diffraction cone. This preparation was done at three different measuring depths (-2 mm, -5 mm and -8 mm) from the weld top surface which represent the center of the three deposited passes each. Consequently, diffraction information were obtained from these positions. As the drill holes for the primary and secondary beam paths require a lot of space, for each sample one single hole was produced for each beam path at a specific measuring depth, only. In the present work we will focus on the strain development in longitudinal direction of the root pass (-8 mm) as well as the final pass (-2 mm) after they were deposited each.

material and welding parameters

Investigations in this work focused on two selected LTT fillers compared to a conventional filler material for high strength steels *(G Mn4Ni2CrMo)* **[30]**. Table 2 shows

their chemical compositions. The LTT alloys differ in their alloying concept. One follows the well-known Cr/Ni filler approach after **[6]**. The other one uses an alternative composition with Mn substituting Ni. The applicability of this modified composition has already been reported **[15]**. With respect to the intended application for low alloyed high strength steels S960QL **[31]** was used as base material *(BM)*. The welding parameters are shown in Table 3. No preheating was applied. To provide the same cooling behavior of each welding layer as well as to avoid unwanted heating of the welding rig between the diffraction experiments and therefore waste of beam time, at the beam line only one welding pass was executed into the gap of the sample. The other welding layers were fabricated in advance of the beam time in the laboratory using the same welding parameters. This procedure allows for cooling to ambient temperature in each case and ensures virtually complete martensite formation.

Temperature measurements were conducted in each weld pass during separate weldments using thermocouples (type K). The measuring positions were chosen similar as to the location of the diffraction gauge volumes, i.e. -2 mm, -5 mm and -8 mm below the weld top surface by immersion of the thermocouples through the primary beam hole (Fig. 3, right). Additionally, at the middle of the sample (x = 60 mm) thermocouples were immersed from the top into the melt during deposition of each pass. Using those measurements the temperature gradient was assessable in combination with the FE model, described in **[29]**. FE revealed that the temperature gradient across the weld metal is ~~neglectable~~ negligible during cooling. So, the measured temperatures are assumed to be representative for each location of diffraction analysis.

Commented [A11]: Due to the word limit of the journal, this sentence was shortened. On the other hand there is one publication dealing with the LTT CrMn only– this is one novel value of this paper (remark of the reviewer 1)

Commented [A12]: Choose different word since immersion normally implies in the presence of a fluid!

Commented [A13R12]: Changed to “hot dipping”.

Commented [A14]: See earlier comment.

Commented [A15R14]: Chenaged to “hot dipping”

Table 2: Chemical composition and material properties of the base and filler materials

Chemical comp. (wt.%),								$R_{p0,2}$	R_m	M_S	B_S
	C	Ni	Cr	Mn	Si	Mo	Fe	MPa	MPa	°C	°C
BM (S960QL)	0.17	0.94	0.49	0.87	0.3	0.52	Bal.	985	1018	419	560
LTT CrNi	0.04	10	10	0.7	0.4	-	Bal.	927	1121	230	-

LTT CrMn	0.08	0.02	11	6.4	0.25	-	Bal.	(-)*	1335	123	-
conventional	0.13	2.19	0.37	1.53	0.8	0.6	Bal.	954	1246	≥ 400	-

M_S, B_S measured in dilatometry test at the base material and pure weld metals
*not determinable, because of no distinctive yield point, elastic area too small

Table 3: welding parameters of the GMAW process for each pass

	LTT CrNi	LTT CrMn	conventional
Wire diameter	1.6 mm		1.2 mm
Voltage	30.8 V		36.8 V
Mean current	343 A		345 A
Welding speed	0.37 m/min		0.45 m / min
Heat input	1,7 kJ*mm^{-1}		
Contact tube distance	18 mm		16 mm
Preheat- and interpass temperature	ambient temperature		
$t_{8/5}$-time (averaged)	12 s		
Welding length	100 mm		
Shielding gas	M21		

data treatment

The procedure is already described in **[19]**. Briefly, with the experimental set-up used, diffraction rings of the lattice planes {200}, {211} and {220} of the martensite phase (α') and the {200}, {220} and {311} of the austenite phase (γ) were evaluated by Bragg's law **[32]**. Using the open-source software "Fit2D" **[33-34]** the Debye-Scherrer-rings that have been recorded at the 2D-detector were integrated. Therefore "Cakes" with an azimuthal angle φ = 15° were defined to obtain a one-dimensional profile of the intensity as a function of 2θ for the longitudinal as well as normal direction according to the weld (see Fig. 3, right). A Pearson-VII-fit was performed for each diffraction peak. By weighting the integrated intensities, $I^{\{hkl\}}$, and using physical factors, ($R^{\{hkl\}}$) **[35-39]**, it is possible to calculate the phase fractions of the austenite (p_γ) and martensite ($p_{\alpha'}$) ~~is calculable~~ based on Equations (1) and (2) with an assumption ~~ing~~ that only those two phases are present **[40-41]**.

$$p_\gamma = \frac{1}{\left[1 + \left(\frac{I_{\alpha'}^{\{hkl\}}}{I_\gamma^{\{hkl\}}} \times \frac{R_\gamma^{\{hkl\}}}{R_{\alpha'}^{\{hkl\}}}\right)\right]} \quad (1)$$

$$p_{\alpha'} = 1 - p_\gamma \quad (2)$$

Commented [A16]: Is this the best terminology for the volume of diffraction?

Commented [A17R16]: I've delegated this questions to the co-authors.

Based on Bragg's law **[32]** the lattice spacings were determined. From that the phase specific unit cell parameter (a_i) was calculated as a function of temperature according to the procedure already described in **[19]**. With a temperature (T) dependent unstrained unit cell parameter ($a_{0,i}$) the elastic strains of the martensite phase (α') and the austenite phase (γ) were calculated using Equation (3).

$$\varepsilon_{i_j} = \frac{a_{i_j}(T) - a_{0,i}(T)}{a_{0,i}(T)}; \text{ i … phase, j … principal direction} \quad (3)$$

The phase specific unstrained unit cell parameter ($a_{0,i}$) was determined experimentally at ambient temperature using stress--relieved combs, which were taken directly from the middle of separate welded samples (x = 60 mm) using identical welding parameters. The total elastic strain (ε_t) was calculated by weighting the elastic strains of the martensite phase ($\varepsilon_{\alpha'}$) and the austenite phase (ε_γ) by their accordant phase fractions using Equation (4).

$$\varepsilon_{t_j}(T) = \varepsilon_{\alpha'_j}(T) \times p_{\alpha'}(T) + \varepsilon_{\gamma_j}(T) \times p_\gamma(T); \text{ j … principal direction} \quad (4)$$

Results and Discussion

microstructure

The microstructure of the welds consists of martensite or bainite and some retained austenite in case of the LTT welds (Fig. 4). Welding of the final pass lead to grain refinement in the root due to multiple heating. All passes exhibit a cellular structure according to the heat flow in normal direction to the weld. Hardness mappings confirmed that the root of the welds becomes tempered while welding of the final pass resulting in hardness gradients towards the HAZ supporting the grain refinement obtained above. In contrast to the LTT CrMn weld the conventional weld and LTT CrNi weld exhibit a homogeneous hardness distribution trough the whole weld.

Commented [A18]: Specify this for the as solidified regions and not the heat affected zones?

Commented [A19R18]: done

Commented [A20]: Is this referring to the cellular structure? How is the cellular structure refined by subsequent weld thermal cycles?

Commented [A21R20]: Thank you for the comment. We think our conclusion was a way too hard. We just would like to say, that tempering was happening in the root.
We deleted the last part of the sentence.
We mentioned a refinement in the root in earlier publications (ref. 43 in the new manuscript)

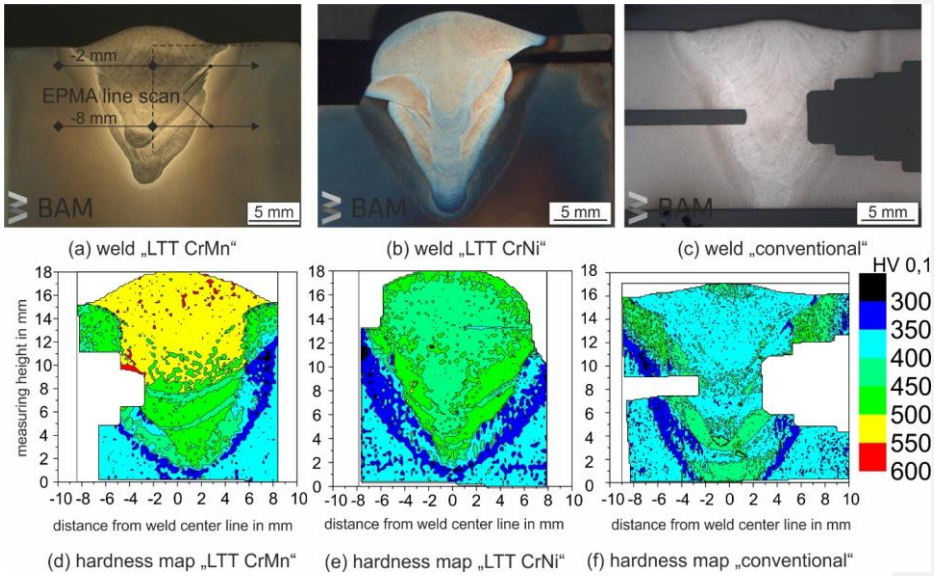

Figure 4: cross section of the joints after welding of the final pass (above) and hardness mappings (below)

As dilution between the LTT welds and the BM was expected additional Electron Probe Micro Analyses (EPMA) were performed at the measuring depths of the in-situ diffraction experiment marked in Fig. 4 (a) using line scans. Measurements of the chemical composition across the welds revealed that the distribution of the main alloying elements Cr, Ni and Mn is characterized by micro segregations. Applying the approach of Steven & Haynes **[42]** allows for an estimation of the M_S and B_S as a function of the main alloying elements. The M_S based on the EPMA analysis across the welds is given in Fig. 5. M_S varies corresponding to the chemical gradient due to dilution with the BM in case of the LTT welds. The distribution of M_S for the conventional weld is unremarkable at 430 °C while B_S keeps constant at 560°C and is therefore not shown. In case of LTT CrNi Ms is 245 °C in average across the final pass and the root. Ms for the LTT CrMn is in average around 120 °C. Nevertheless, both root welds are characterized by a higher variation (up to +100K). Therefore, localized higher Ms temperatures are

Commented [A22]: How did the authors accommodate the microsegregation (as stated in an earlier statement.)

Commented [A23R22]: Microsegregation was proven in ealierer publications by Electron probe micro analyses. We added the publication in the ealierer statement.
In this publication we were focussing on line scans using WDX, we added Table 4 with the parameters used.

expected when welding the root. The transition from the weld metal into the HAZ shows in both cases an abrupt rise of Ms. A M_S of 420 °C are found here independent of the LTT weld metal.

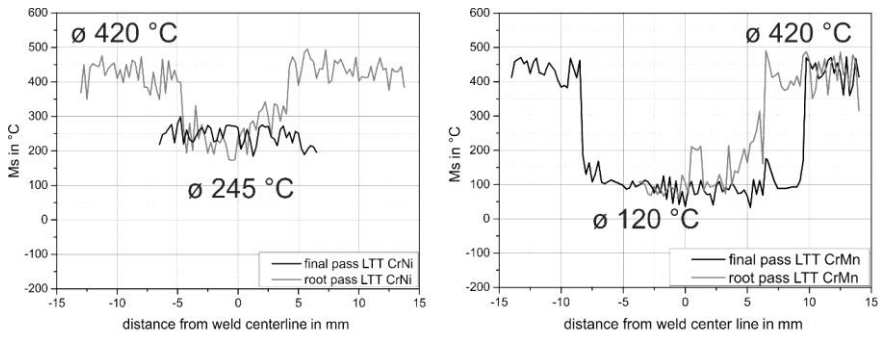

Figure 5: M_S distribution over the cross section of the LTT CrNi weld (left) and LTT CrMn weld (right) based on EPMA analyses of the chemical composition and the empirical approach of Steven and Haynes [42]

Commented [A24]: What is the meaning of the symbol (crossed O) before temperature?

Commented [A25R24]: Average temperatures of the HAZ and the weld. We've changed the cutline

Martensite and bainite formation

Fig. 6 shows the formation of martensite (α') and bainite (α_b) during cooling of the root (left) and of the final passes (right) of the LTT as well as for the conventional weld metals after deposition. In case of root welding the first α diffraction signals of the conventional weld started to appear already above 550 °C. Those first signals are likely to be related to the formation of bainite. During cooling α' appears subtly at 420 °C. At ambient temperature about 95% of α_b and α' were formed in sum. In case of LTT the α' phase started to appear also at 420 °C. No bainite was observed. As the observed Ms matches well with the estimation following Steven & Haynes based on the EPMA analyses it is assumed that the signal at 420 °C stemmed from the transition area into the HAZ which is part of the gauge volume.

A short saturation was found when 7% - 10% α' were formed. The characteristic Ms of the LTT CrNi weld metal was then situated at 360 °C while Ms of LTT CrMn was

Commented [A26]: Why is this saturation? Explain!

found at 327 °C. These temperatures correspond with the maximum variance of Ms calculated by Steven & Haynes (Fig. 5). During further cooling the martensite phase fraction development was comparable between the LTT welds CrNi and CrMn until ambient temperature was reached. Finally, in both cases around 95% of martensite similar to the conventional filler material were formed. Worth mentioning the maximum formation rate of α' was reached at 55% independent from the filler material used.

Comparable to the root α_b and α' phase fraction of the conventional weld started to increase from already about 550 °C for the final pass. An additional change in slope became visible at around 380 °C. While the first inflection point corresponds to the known formation of bainite, the second one is assumed to belong to martensite. After cooling to ambient temperature about 92% of α_b and α' phase were formed. The same accounts for the amount of α' phase of LTT CrNi. Here solely martensite starts to appear at 210 °C. LTT CrMn shows an M_S of approximately 170°C. Both temperatures are fairly comparable to the analytical estimation (Fig. 5). It is interesting that LTT CrMn martensite was formed more rapidly compared the LTT CrNi. While 50% of martensite of the latter were formed in a temperature range of $\Delta T = 70$ °C, the LTT CrMn had formed the same amount of martensite already in a range of $\Delta T = 50$ °C. The amounts of retained austenite at ambient temperature are below 10% for the conventional wire and LTT CrNi, respectively below 17% of LTT CrMn.

In summary the LTT fillers show lower Ms temperatures than the conventional filler material. In case of the LTT root welds dilution with the BM induces a shift of Ms to higher temperatures compared to the nominal values. Nevertheless, the martensite formation is virtually completed at ambient temperature. Less dilution is observed for the final pass. Here Ms of LTT is in the expected temperature range. Martensite formation is

Commented [A27]: How does dilution increase Ms temperature? Dilution would increase carbon content which is expected to lower Ms temperature.

Commented [A28R27]: You are right, a higher carbon content will decrease the Ms.
On the one hand, the carbon contetnt in the base amterial is quite low and therefore the mixing is not too high. On the other hand, the combustion and dilution of the alloying elements Mn, Cr and Ni with the base material is dominant, so that the Ms will be increased.

more rapid here compared to the root due to lower segregation across the weld. LTT CrMn is characterized by low amounts of retained austenite at ambient temperature.

Commented [A29]: As Ms temperature is lower, then would retained austenite not be expected to increase?

Commented [A30R29]: This depends on the martensite-finish-temperature (Mf). Depending on the dilution of the weld Mf of the LTT CrMn is close to ambient temperature. Retained austenite was found at the detection limit of the analyses only

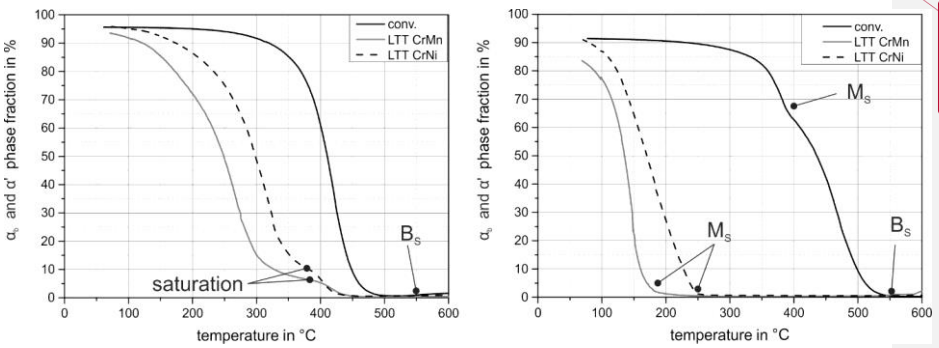

Figure 6: development of the α and α' phase fraction during cooling after welding of the root pass (left, measuring depth = -8 mm) and after welding of the final pass (right, measuring depth = -2 mm)

Macroscopic strain during cooling

The macroscopic strain was calculated after Equation (4) as a function of the phase specific strains taking into account the amount of each phase fraction. Fig. 7 shows the development of the macroscopic strains after welding of the root (left) as well as of the final pass (right) during cooling in longitudinal direction of the weld. In case of the root at high temperatures around 600 °C the strain of the conventional weld started in compression and was increased to around $\varepsilon_t = -1*10^{-3}$ during cooling until M_S was reached. The phase transformation into bainite at 550 °C was not effective on the strain. After Ms = 420 °C the strain stayed constant approximately between $\varepsilon_t = 0$ and $\varepsilon_t = -1*10^{-3}$. The strain induced by hindered shrinkage and that induced by phase transformation were balancing each other until ambient temperature was reached.

Contrary to that high temperature tensile strains up to $\varepsilon_t = 3*10^{-3}$ were observed above Ms in case of the LTT weld metals in absence of bainite formation due to restrained shrinkage. The first martensite formation at 420 °C (transition to HAZ) counteracts the

shrinkage and kept the strain at an almost constant level between $\varepsilon_t = 1*10^{-3}$ and $\varepsilon_t = 3*10^{-3}$. After Ms of the LTT weld metals was reached at 360 °C for LTT CrNi and 327 °C for LTT CrMn the strains decreased from tension to compression with ongoing martensite formation. At ambient temperature compressive strains comparable (respectively below for LTT CrMn) to the conventional weld are present. Despite different initial strain levels, the low-temperature martensitic transformation in the LTT welds ensures that comparable strain levels are present at ambient temperature.

Investigating the final pass (Fig. 7, right), the strain formation of the conventional weld was comparable to that of the root in quality. As in case of the root the influence of the bainite phase transformation on the strain was negligible. Tensile~~on~~ strain rised up to $\varepsilon_t = 1.6*10^{-3}$ due to restrained shrinkage. When reaching M_S of the weld, the total tensile~~on~~ strain was slightly reduced to $\varepsilon_t = 1.3*10^{-3}$. During further cooling the strain was balanced at $\varepsilon_t = 1.1*10^{-3}$ until ambient temperature was reached. In contrast to the root, the total strain of the final pass is tensile for the conventional weld. In case of the LTT welds the strains of the final pass do not increase significantly during cooling. The strains are balanced at constant levels. While LTT CrNi is in compression around $\Delta\varepsilon = -0.5*10^{-3}$, LTT CrMn is tensile at the same level as the conventional weld. Nevertheless, when Ms at 185 °C was reached, the strain was quickly pushed into compression by the newly formed martensite to $\varepsilon_t = -1.5*10^{-3}$. This continued until ambient temperature. In the LTT CrNi weld the strain is decreased after Ms was reached at 248 °C exactly to the same level. Therefore, at ambient temperature the amount of compressive strain is similar between the LTT welds at $\varepsilon_t = -1.5*10^{-3}$.

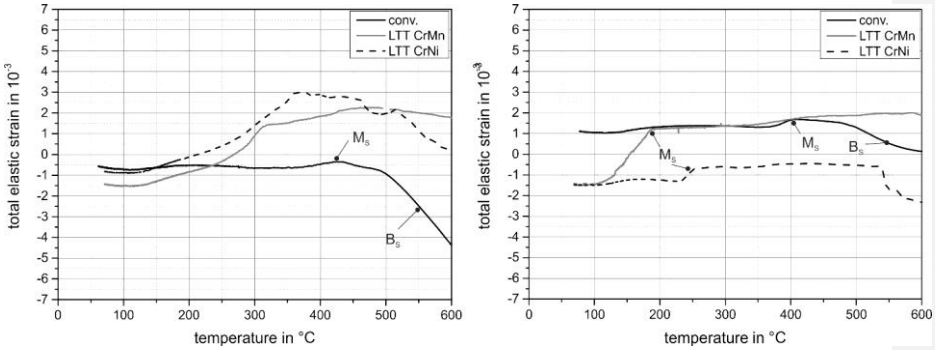

Figure 7: total elastic strain development of the LTT CrNi, LTT CrMn and conventional weld in longitudinal direction after welding of the root (left, measuring position at "-8 mm" in the root pass) and after welding of the final pass (right, measuring position "-2 mm" in the final pass)

While the difference of the total elastic strain in the root was low between the filler materials investigated, the strain level of the final pass was much more influenced by the LTT filler materials. In contrast to the conventional weld compressive strains w~~h~~ere formed here. Despite that the LTT CrNi behaved differently compared to LTT CrMn. Therefore, phase specific strains of austenite and martensite are discussed separately in the following.

Phase specific strain during cooling - root

Fig. 8 shows the phase specific strain development of the γ (left) and α_b and α' phase (right) found during cooling of the root in longitudinal direction. The level of strain in the austenite phase differs at 600 °C. While the conventional weld is in compression the LTT ones are in tension. Due to restrained shrinkage the austenite strain increased towards tension in all cases. The martensite phase transformation at 420°C balanced the strain level or even decreased it somewhat in the conventional case. The bainite phase transformation had no influence on the remaining austenite strain. During further cooling the austenite strain in the conventional weld kept growing and resulted in tension at

Commented [A31]: Consistency: Some sub headings are capitalized, others are not.

Commented [A32R31]: Ok thank you

ambient temperature. Contrary to that the strain in the LTT welds is reduced when their specific Ms' were reached. LTT CrMn austenite was more ~~effected~~affected. The strain continuously decreased down to ambient temperature showing a compressive strain of $\varepsilon_\gamma = -1.5*10^{-3}$. The LTT CrNi and the conventional weld resulted both in tension strain to about $\varepsilon_\gamma = 2*10^{-3}$.

In case of the α_b and α' strain evolution remarkable compression strains were detected at a temperature of 600 °C for all filler materials investigated. Nevertheless, the phase fraction of the α_b and α' phase was too low to influence the total strain (Fig. 7). Note, that α diffraction signals were already detectable above bainite start. These very weak signals are assumed to stem from very ~~few~~ small amounts of ferrite which are not considered here. During further cooling the compression strain decreases due to restrained shrinkage until M_S at 420 °C. The ongoing martensite formation in the conventional case then counteracted the shrinkage balancing the strain at a constant level. At ambient temperature a strain of approximately $\varepsilon_{\alpha'} = -0.5*10^{-3}$ was observed. For the LTT welds the martensite formed at 420°C is limited to a small amount (7% - 10%, see Fig. 6) in the transition to the HAZ. Therefore, high tensile strains found in the austenite at the same time rised the martensite strain abruptly into tension. Reaching the characteristic Ms of each LTT weld metal the strains are continuously decreased until ambient temperature to a similar level as found for the conventional weld. The phase specific strains in the root illustrate that the amount of martensite formed is crucial for counteracting shrinkage induced strains. Too low amounts of martensite do not affect the austenite strain. Then the total strain is ruled by the austenite.

Commented [A33]: Unclear what the meaning of transition to HAZ? Is that because of the prior weld being heat treated by subsequent weld thermal cycle?

Commented [A34R33]: Ok; we would like to say, that the first LTT martensite formed (7%-10%) is caused by the region of the weld, which is very close to the HAZ. This is due to an increase of the Ms in this region.

We changed this sentence a little bit.

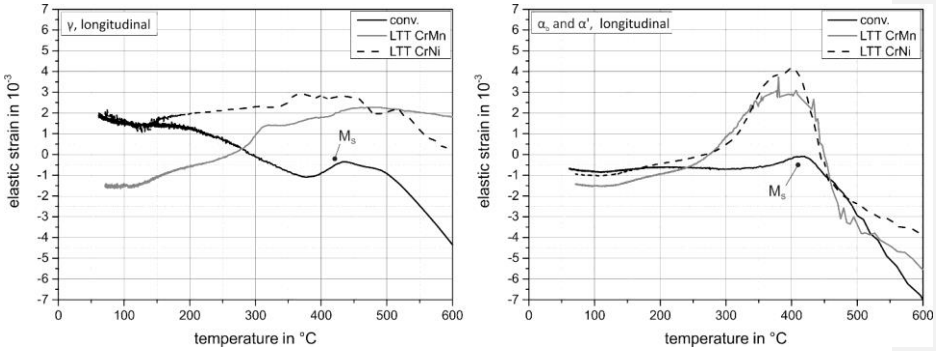

Figure 8: Phase specific strain evolution in longitudinal direction of the y phase (left) and the α_b and α' phase (right) during cooling of the root weld (z = -8 mm)

Phase specific strain during cooling – final pass

Fig. 9 shows the phase specific strain development of the γ (left) and α_b and α' phase (right) found during cooling of the final pass in longitudinal direction. In quality the strain development in the conventional weld is similar to the root. However, the strain level is shifted to tensile values. This accounts for austenite as well as for martensite (and bainite). The martensite formation barely affected the austenite which resulted in high tensile strains above $\varepsilon_\gamma = 5*10^{-3}$. The martensite itself shows a quiet constant tensile strain level during cooling to ambient temperature below $\varepsilon_{\alpha'} = 1*10^{-3}$.

In contrast to the conventional weld the austenite strain of the LTT welds was decreased when the specific M_S of the weld metals was reached. At ambient temperature compression strain was found around $\varepsilon_\gamma = -2*10^{-3}$. The martensite strain in the LTT weld metals behaved different compared to the root. LTT martensite is the first α diffraction signal in absence of any HAZ related martensite/bainite/ferrite as found for the root. Therefore, the first martensite strain values are highly compressive around $\varepsilon_{\alpha'} = -6.5*10^{-3}$ independent from the LTT filler investigated. With increasing amount of martensite the strain quickly raised up to about $\varepsilon_{\alpha'} = -1*10^{-3}$. After 50% of martensite had formed the strain suddenly stayed nearly constant at that level down to ambient temperature. Further

Commented [A35]: What is the meaning of a quiet constant tensile strain?

Commented [A36R35]: The word is "quite" We replaced it with "nearly"

Commented [A37]: Further speculate or elaborate on why the 50% martensite "thereshold".

Commented [A38R37]: We've added some further elaborations.

We think this due to the fact, that the evolution of martensite is associated with compressive strain. During cooling, the strain level of the first 50% is influenced and dominated by the shrinkage restraint. For this specific sample after 50% of martensite have formed, the phase transformation is dominant then, counteracting the shrinkage induced strain. On the other hand the shrinkage restraint will be lower due to a smaller temperature gradient. We are looking forward to investigate that.

increase of the martensite phase fraction due to ongoing martensite phase transformation counteracts the strain development induced by shrinkage restraint.

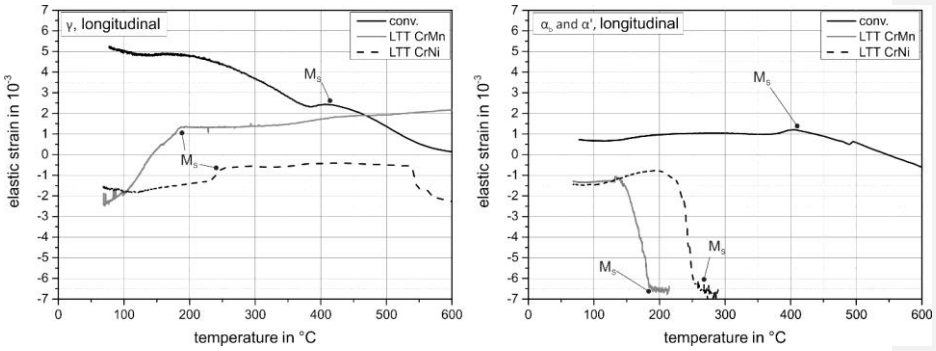

Figure 9: Phase specific strain evolution in longitudinal direction of the y phase (left) and the α_b and α' phase (right) during cooling of the final pass of the weld (z = -2 mm)

Comparable to the root the characteristic martensite formation in the LTT welds of the final pass induced high compressive strains. But in case of the root the strain is an accumulated signal containing diluted areas of the HAZ (see Fig. 5) next to the pure weld metal. In consequence the strains found for the root smear the "LTT effect". The evaluation of the efficiency of LTT fillers should therefore be based on the final pass. In principle the theoretical model of stress formation during cooling of a weld metal undergoing phase transformation after Nitschke-Pagel and Wohlfahrt **[4]** was proven in the present study. Even more an in-situ diffraction experiment allowing for a separation of the strain in austenite and martensite was realized.

Using LTT filler materials the total elastic strain was reduced compared to the conventional weld but dilution must carefully be considered. Due to the lower M_S of the LTT filler materials, ~~tension~~ tensile strain of the austenite was decreased to compression while for the conventional weld restrained shrinkage led to tensile strains. In contrast to the conventional weld delayed and ongoing martensite phase transformation of the LTT weld led to compressive strains for the martensite phase. Worth mentioning, also in the

conventional weld the undergoing martensite formation could balance the shrinkage induced strains to a certain degree**.**

Summary and Conclusions

In-situ diffraction analysis during GMAW was conducted to observe the effect of martensite formation on the phase specific strains developed during cooling. Two LTT filler materials were compared to a conventional high strength filler. From the results obtained, the following conclusions can be drawn:

- M_S varies in case of the LTT joints over the weld cross section due to dilution of the weld with the heat affected zone. For the sample used, this is most pronounced for the root as the contact area between weld metal and base material is larger. Depending on the amount of dilution also the content of the phase fractions was slightly altered.
- Despite a high restraint intensity the total elastic strain in longitudinal direction was reduced by delayed martensite formation using LTT filler materials. The volume expansion due to the martensite phase transformation counteracted the strains formed by restrained shrinkage. In case of the final pass even compression strain was achieved for the LTT welds while the conventional weld was in tension.
- The martensite phase transformation decreased the strain of the austenite. While this effect is leading to compression strain in case of the LTT welds the austenite of the conventional weld carries still tension strain during cooling.
- High compressive strains were suddenly present in the martensite phase when Ms was reached. The strains decreased quickly due to restrained shrinkage but stayed in compression at ambient temperature and for the final pass.

- Both LTT fillers (Ms = 230 °C and Ms = 123 °C) used in this study show similar strain formation during cooling despite different transformation temperatures. But due to the pronounced dilution with the base material Ms in the root weld is raised compared to these nominal values. This must be considered when choosing the type of LTT filler.

Acknowledgements

Parts of this research were carried out at the light source PETRA III at DESY, a member of the Helmholtz Association (HGF). We would like to thank Torben Fischer for assistance in using beamline P07. The authors would like to especially acknowledge the German Research Foundation (DFG) for funding parts of this work (KA 1807/4-1 | GI 376/4-1), Lincoln Electric Europe for provision of welding consumables as well as EWM AG for support.

References

[1] Karlsson L.: Thermal Stresses in Welding: Thermal Stresses I. Amsterdam (NLD): Elsevier Science Ltd; 1986: 299–389

[2] Bretz W, Hoffmeister H. Effect of hydrogen, restraint and welding conditions on weld metal cold cracking of HSLA steels in the IRC test. mater technol. 1987;58(3):142–147

[3] Heeschen J, Wohlfahrt H. Residual Stresses in Science and Technology: Assessment of the Influence of Shot Peening on the Fatigue Strength of Butt Welded Joints. Oberursel (GER): DGM Informationsgesellschaft Verlag; 1987:467-476

[4] Nitschke-Pagel T, Wohlfahrt H. Residual Stresses in Welded Joints - Sources and Consequences. mater sci forum. 2002;404-407:215-226

[5] Jones W K C, Alberry P J. Residual stresses in welded construction and their effects: A model for stress accumulation in steel during welding. British Weld Res Association; 1978:15–26

[6] Ohta A, Watanabe A, Matsuoka K, et al. fatigue strength improvement by using newly developed low transformation temperature welding material. weld world. 1999;43(6):38-42

[7] Wang W,Huo L, Zhang Y, et al. New Developed Welding Electrode for Improving the Fatigue Strength of Welded Joints. J mater sci & technol. 2002;18(6):527–531

[8] Kromm A, Dixneit J, Kannengiesser T. Residual stress engineering by low transformation temperature alloys-state of the art and recent developments. Weld world. 2014;58(5):729-741
[9] Bhadeshia H K D H, Street P, Cb C. Developments in Martensitic and Bainitic Steels : Role of The Shape Deformation Materials Science and Metallurgy. mater sci & eng A. 2004;A378:34–39
[10] Dai H, Francis J A, Stone H J, et al. Characterizing phase transformations and their effect on ferritic weld residual stresses with X-rays and neutrons. metall mater trans A. 2008;39:3070–3078
[11] Shiga C, Yasuda H Y, Hiraoka K, et al. Effect of Ms temperature on residual stress in welded joints of high-strength steels. Weld World. 2010;54:71–79
[12] Kromm A, Kannengiesser T, Altenkirch J, et al. Residual Stresses in Multilayer Welds with Different Martensitic Transformation Temperatures Analyzed by High-Energy Synchrotron Diffraction. mater sci forum. 2011;681:37-42.
[13] Ramjaun T, Stone H J, Karlsson L, et al. Effect of interpass temperature on residual stresses in multipass welds produced using low transformation temperature filler alloy. sci technol weld join. 2014;19(1):44-51
[14] Dixneit J, Kromm A, Boin M, et al. Influence of Heat Control on Residual Stresses in Low Transformation Temperature (LTT) Large Scale Welds. mater res proc (ICRS-10). 2016;2:223–228.
[15] Kromm A.: Evaluation of weld filler alloying concepts for residual stress engineering by means of Neutron and X-ray diffraction. adv mater res-switz. 2014;996:469-474
[16] Gibmeier J, Obelode E, Altenkirch J, et al. Residual stress in steel fusion welds joined using low transformation temperature (LTT) filler material. mater sci forum. 2014;768-769:620-627
[17] Kromm A, Kannengiesser T. Effect of martensitic phase transformation on stress build-up during multilayer welding. mater sci forum. 2014;768-769:660-667
[18] Altenkirch J, Gibmeier J, Kromm A, et al. In situ study of structural integrity of low transformation temperature (LTT)-welds. mat sci & eng A. 2011;528(16-17):5566-5575
[19] Altenkirch J, Gibmeier J, Kostov V, et al. Time- and temperature-resolved synchrotron X-ray diffraction: observation of phase transformation and strain evolution in novel low temperature transformation weld filler materials. The J of Strain Analysis for eng des. 2011;46(7):563–579
[20] Gibmeier J, Held E, Altenkirch J, et al. Real time monitoring of phase transformation and strain evolution in LTT weld filler material using EDXRD. J of mater process technol. 2014;214(11):2739–2747
[21] Kromm A, Kannengiesser T, Gibmeier J: In-Situ Observation of Phase Transformations during Welidng of Low Transformation Temperature Filler Material. mater sci forum. 2010;638-642:3769-3774
[22] Satoh K, Ueda Y, Matsui S, et al. Japanese studies on structural restraint severity in relatio to weld cracking (Preliminary report). weld world. 1977;15(7/8):155–162
[23] Kromm A, Rhode M, Kannengiesser T: Influence of heat control on welding residual stresses in multi-layer component joints. In: Babu S, Bhadeshia H K D H, Cross C E, et al., editors. Trends in welding research - Proceedings of the 9th international conference; 2013; Chicago (IL, USA), p. 48-54
[24] Francis J A, Smith M C, Jeyaganesh B, et al. Design and Manufacture of Industrially Representative Weld Mock-ups for the Quantification of Residual

Stresses in a Nuclear Pressure Vessel Steel. mater res proc (ICRS-10). 2016;2:581–586
[25] Dai H, Moat R J, Withers P J: Modelling the interpass temperature effect on residual stress in low transformation temperature stainless steel welds. In: ASME PRESSURE VESSELS AND PIPING CONFERENCE. 2011;6(Part B):1451–1458). Baltimore (MD, USA).
[26] Gadallah R, Murakawa H. Numerical Study on Influence of Specimen Size upon Welding Residual Stress. In: Visual-JW The International Symposium on Visualization in Joining & Welding Science through Advanced Measurements and Simulation; 2014; Osaka (JPN) p. 324–325
[27] Schell N, King A, Beckmann F, et al. The High Energy Materials Science Beamline (HEMS) at PETRA III. mater sci forum. 2013;772:57–61
[28] Schwenk C, Kannengiesser T, Rethmeier M: Restraint Conditions and Welding Residual Stresses in Self-Restrained Cold Cracking Tests. In: Trends in Welding Research, Proceedings of the 8th International Conference; 2008 June 1-6; Callaway Gardens Resort, Pine Mountain (GA, USA)
[29] Weidemann J, Dixneit J, Kromm A, et al. INFLUENCE OF STRUCTURAL STIFFNESS ON THE RESIDUAL STRESSES DURING WELDING OF LOW TRANSFORMATION TEMPERATURE ALLOYS. In: Sommitsch C, Enzinger N, Mayr, P. editors. Mathematical Modelling of Weld Phenomena 11. Proceedings of the 11th International Seminar Numerical Analysis of Weldability. 2015; Seggau (AUT) 2016. p. 259–276
[30] International Organization for Standardization. Welding consumables - Wire electrodes, wires, rods and deposits for gas shielded arc welding of high strength steels – Classification. 2012. Standard No. DIN EN ISO 16834
[31] European Standardization. Hot rolled products of structural steel – Part 6: Technical delivery conditions for flat products of yield strength structural steels in the quenched and tempered condition. 2004. Standard No. DIN EN 10025-6
[32] Bragg W: The reflection of x-rays by crystals. Proceedings of the Royal Society of London. 1913;Series A:428-438
[33] Hammersley A P. FIT2D: An Introduction and Overview. 1997. (*ESRF Internal Report*, ESRF97HA02T)
[34] Hammersley A P, Svensson S O, Hanfland M, et al. Two-Dimensional Detector Software: From Real Detector to Idealised Image or Two-Theta Scan. High press res. 1996;14:235-248
[35] Laine E S U: A high-speed determination of the volume fraction of ferrite in austenitic stainless steel by EDXRD. J of Physics F: Metal Physics, 1978;8(7):1343–1348
[36] Darken L S; Smith R P. Thermodynamic Functions of Iron. ind and eng chem. 1951;43(8):1815–1820
[37] Chantler C T: Theoretical Form Factor, Attenuation, and Scattering Tabulation for Z=1–92 from E = 1–10 eV to E = 0.4–1.0 MeV. J. physics. chem. ref. data. 1995;24(1):71–643
[38] Chantler C T, Olsen K, Dragoset R A; et al. X-Ray Form Factor, Attenuation, and Scattering Tables. NIST database. 2001
[39] Daymond M R: The determination of a continuum mechanics equivalent elastic strain from the analysis of multiple diffraction peaks. J of appl physics. 2009;96(8):4624–4272
[40] Macherauch E; Zoch H-W: Praktikum in Werkstoffkunde 91 ausführliche Versuche aus wichtigen Gebieten der Werkstofftechnik [practical training in

material science 91 experiments from the most important fields of material science]. Wiesaden (DEU): Vieweg+Teubner Verlag; 2011. p. 114. in german
[41] Spieß L, Teichert G, Schwarzer R, et al. Moderne Röntgenbeugung. Röntgendiffraktormetrie für Materialwissenschaftler, Physiker und Chemiker [modern x-ray diffraction. x-ray diffraction for material scientists, physicists and chemists]. Wiesbaden (DEU): Vieweg+Teubner Verlag; 2009, p. 241. in german
[42] Steven W, Haynes A G. The temperature of formation of martensite and bainite in low-alloy steels. J Iron Steel Inst. 1956;183(8):349–359

listing of the revisions made in the paper

Ref.: STW4710
real time assessment of the strain evolution during GMA welding of low transformation temperature filler materials (LTT)

Revisions made:

1. Change of the heading of the paper. We would like to avoid that potential readers expect the results to be presented over time.
2. We have added a further author of the paper: Mr. Torben Fischer. He was the responsible beam line scientist during our measurements. He was helping us to analyze the raw data. Please consider him.
3. The abstract was revised
4. The original figure 1 in the chapter “state of the art” of the paper was removed due to the word limit of the journal. Furthermore, there was no added value in terms of content from the former figure 1
5. The hardness mappings in the original figure 4 have been removed. The values are now in the text, only. The presentation was not relevant for the conclusions in the paper. Thereby it was possible for us to reduce the number of words.
6. All other figures were improved in the clarity only.
7. The description of the sub-chaper “data treatment in the chapter “Experimental” was explained in more detail in order to make the elaboration of the raw data more transparent for the reader
8. In the chapter “Experimental” the sub-chapter “Miscellaneous” was added
9. Some text passages have been linguistically revised
10. The conclusions have been revised

With kind regards

Jonny Dixneit